Immunity

The RNA editor ADAR2 promotes immune cell trafficking by enhancing endothelial responses to interleukin-6 during sterile inflammation

Graphical abstract

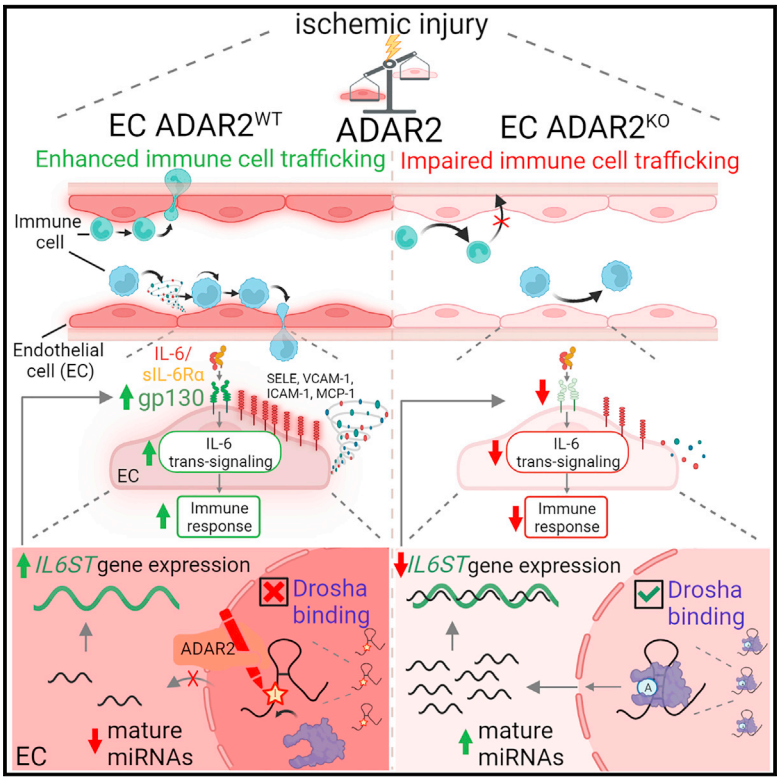

Highlights

- The RNA editor ADAR2 safeguards gp130 expression by reprograming RNAi circuits
- ADAR2 is required for vascular endothelial immune responses to IL-6
- Immune cell trafficking in ischemic tissues is promoted by IL-6 *trans*-signaling
- Hypoxia-induced ADAR2 enhances immune cell trafficking in areas of ischemic injury

Authors

Aikaterini Gatsiou, Simon Tual-Chalot, Matteo Napoli, ..., Markus Sperandio, Oliver Soehnlein, Konstantinos Stellos

Correspondence

aikaterini.gatsiou@newcastle.ac.uk (A.G.), konstantinos.stellos@medma.uni-heidelberg.de (K.S.)

In brief

Immune cell trafficking is integral for organism resilience to stress, but how the vascular endothelium adjusts this process to environmental stimuli remains elusive. Gatsiou et al. report that RNA nucleotide changes made by the hypoxia-induced RNA editor ADAR2 promote endothelial responses to IL-6 that enhance leukocyte trafficking in ischemic tissues.

Gatsiou et al., 2023, Immunity *56*, 979–997
May 9, 2023
https://doi.org/10.1016/j.immuni.2023.03.021

CellPress

Immunity

CellPress
OPEN ACCESS

Article

The RNA editor ADAR2 promotes immune cell trafficking by enhancing endothelial responses to interleukin-6 during sterile inflammation

Aikaterini Gatsiou,[1,2,*] Simon Tual-Chalot,[1,33] Matteo Napoli,[3,33] Almudena Ortega-Gomez,[4,34,36] Tommy Regen,[5,34] Rachit Badolia,[6,34] Valeriana Cesarini,[7,34] Claudia Garcia-Gonzalez,[8] Raphael Chevre,[4,9] Giorgia Ciliberti,[10] Carlos Silvestre-Roig,[4,9] Maurizio Martini,[11,12] Jedrzej Hoffmann,[13] Rana Hamouche,[6] Joseph R. Visker,[6] Nikolaos Diakos,[6] Astrid Wietelmann,[8] Domenico Alessandro Silvestris,[7] Georgios Georgiopoulos,[14,25]

(Author list continued on next page)

[1]Biosciences Institute, Vascular Biology and Medicine Theme, Faculty of Medical Sciences, Newcastle University, Newcastle upon Tyne, UK
[2]RNA Metabolism and Vascular Inflammation Laboratory, Institute of Cardiovascular Regeneration and Department of Cardiology, JW Goethe University Frankfurt, Frankfurt am Main, Germany
[3]Institute for Cardiovascular Physiology and Pathophysiology, Walter Brendel Center for Experimental Medicine Biomedical Center (BMC), Ludwig-Maximilians-Universität München, Munich, Germany
[4]Institute for Cardiovascular Prevention (IPEK), LMU Munich Hospital, Munich, Germany
[5]Institute for Molecular Medicine, University Medical Center of the Johannes Gutenberg University of Mainz, Mainz, Germany
[6]Nora Eccles Harrison Cardiovascular Research and Training Institute (CVRTI), University of Utah School of Medicine, Salt Lake City, UT, USA
[7]Department of Pediatric Hematology/Oncology and Cellular and Gene Therapy, Bambino Gesù Children's Hospital, IRCCS, Rome, Italy
[8]Max-Planck Institute for Heart and Lung Research, Bad Nauheim, Germany
[9]Institute for Experimental Pathology (ExPat), Center for Molecular Biology of Inflammation, WWU Muenster, Muenster, Germany
[10]Department of Cardiovascular Research, European Center for Angioscience (ECAS), Heidelberg University, Mannheim, Germany
[11]Fondazione Policlinico Universitario "A. Gemelli," IRCCS, UOC Anatomia Patologica, Rome, Italy
[12]Istituto di Anatomia Patologica, Università Cattolica del Sacro Cuore, Rome, Italy
[13]Department of Cardiology, Goethe University Hospital Frankfurt, Frankfurt am Main, Germany
[14]Department of Clinical Therapeutics, Alexandra Hospital, National and Kapodistrian University of Athens Medical School, Athens, Greece
[15]Kancera AB, Stockholm, Sweden
[16]Department of Oncology and Pathology at Karolinska Institutet, Stockholm, Sweden
[17]Department of Biology, Southern University of Science and Technology, Shenzhen, Guangdong, China

(Affiliations continued on next page)

SUMMARY

Immune cell trafficking constitutes a fundamental component of immunological response to tissue injury, but the contribution of intrinsic RNA nucleotide modifications to this response remains elusive. We report that RNA editor ADAR2 exerts a tissue- and stress-specific regulation of endothelial responses to interleukin-6 (IL-6), which tightly controls leukocyte trafficking in IL-6-inflamed and ischemic tissues. Genetic ablation of ADAR2 from vascular endothelial cells diminished myeloid cell rolling and adhesion on vascular walls and reduced immune cell infiltration within ischemic tissues. ADAR2 was required in the endothelium for the expression of the IL-6 receptor subunit, IL-6 signal transducer (IL6ST; gp130), and subsequently, for IL-6 *trans*-signaling responses. ADAR2-induced adenosine-to-inosine RNA editing suppressed the Drosha-dependent primary microRNA processing, thereby overwriting the default endothelial transcriptional program to safeguard gp130 expression. This work demonstrates a role for ADAR2 epitranscriptional activity as a checkpoint in IL-6 *trans*-signaling and immune cell trafficking to sites of tissue injury.

INTRODUCTION

Adenosine-to-inosine (A-to-I) RNA editing is an epitranscriptional modification essential for life,[1–3] catalyzed by the adenosine deaminases acting on RNA-1 and -2 (ADAR1 and ADAR2) in mammals[4,5] and can effectively change the fate of RNA molecules. Despite being the first RNA modification to be biologically explored, the functional consequences of the millions of edited positions[6,7] remain greatly unexplored (reviewed in Quin et al.,[8] Eisenberg and Levanon,[9] Walkley and Li,[10] and Nishikura[11]). Brain and vascular tissues are among the most highly edited tissues.[6] However, previous research has mostly focused on the

Ali Moshfegh,[15,16] Andre Schneider,[8] Wei Chen,[17,18] Stefan Guenther,[8] Johannes Backs,[19,20] Shin Kwak,[21] Craig H. Selzman,[6,22] Kimon Stamatelopoulos,[14,25] Stefan Rose-John,[23] Christian Trautwein,[24] Ioakim Spyridopoulos,[25,26] Thomas Braun,[8,35] Ari Waisman,[5,35] Angela Gallo,[7,35] Stavros G. Drakos,[6,27,35] Stefanie Dimmeler,[28,30,35] Markus Sperandio,[3,31] Oliver Soehnlein,[4,9,31,32] and Konstantinos Stellos[1,2,10,20,29,37,*]

[18]Medi-X Institute, SUSTech Academy for Advanced Interdisciplinary Studies, Southern University of Science and Technology, Shenzhen, Guangdong, China
[19]Institute of Experimental Cardiology, University Hospital Heidelberg, Heidelberg, Germany
[20]German Centre for Cardiovascular Research (Deutsches Zentrum für Herz-Kreislauf-Forschung, DZHK), Heidelberg/Mannheim Partner Site, Heidelberg and Mannheim, Germany
[21]Department of Molecular Neuropathogenesis, Tokyo Medical University, Tokyo, Japan
[22]Division of Cardiothoracic Surgery, University of Utah School of Medicine, Salt Lake City, UT, USA
[23]Institute of Biochemistry, Christian-Albrechts-University Kiel, Kiel, Germany
[24]Department of Internal Medicine III, University Hospital RWTH Aachen, Aachen, Germany
[25]Translational Research Institute, Vascular Biology and Medicine Theme, Faculty of Medical Sciences, Newcastle University, Newcastle upon Tyne, UK
[26]Department of Cardiology, Freeman Hospital, Newcastle upon Tyne NHS Foundation Trust, Newcastle upon Tyne, UK
[27]Division of Cardiovascular Medicine, University of Utah School of Medicine, Salt Lake City, UT, USA
[28]Institute of Cardiovascular Regeneration, Center of Molecular Medicine, JW Goethe University Frankfurt, Frankfurt am Main, Germany
[29]Cardio-Pulmonary Institute (CPI), Frankfurt am Main, Germany
[30]German Centre for Cardiovascular Research (Deutsches Zentrum für Herz-Kreislauf-Forschung, DZHK), Frankfurt Partner Site, Germany
[31]German Centre for Cardiovascular Research (Deutsches Zentrum für Herz-Kreislauf-Forschung, DZHK), Munich Heart Alliance Partner Site, Munich, Germany
[32]Department of Physiology and Pharmacology (FyFa), Karolinska Institutet, Stockholm, Sweden
[33]These authors contributed equally
[34]These authors contributed equally
[35]These authors contributed equally
[36]Present address: Department of Endocrinology and Nutrition, Virgen de la Victoria Hospital, Institute of Biomedical Research in Malaga (IBIMA), Malaga University, Malaga, Spain
[37]Lead contact
*Correspondence: aikaterini.gatsiou@newcastle.ac.uk (A.G.), konstantinos.stellos@medma.uni-heidelberg.de (K.S.)
https://doi.org/10.1016/j.immuni.2023.03.021

importance of A-to-I RNA editing in brain tissues and diseases,[12] while its role in vascular tissues and especially in vascular endothelium remains poorly understood (discussed in Gatsiou and Stellos).[13] To date, most studies examined the function of ADAR1, but not of ADAR2, since ADAR1 catalyzes the vast majority of RNA editing events.[14–18] The main physiological function of the less studied ADAR2 is attributed to the exonic RNA editing of the neuronal glutamate receptor (GluR), a process that is essential for neuronal homeostasis.[3]

Immune cell trafficking constitutes a fundamental biological process, facilitating the access of effector cells to sites of tissue injury or inflammation. Vascular endothelial cells (ECs) are the gatekeepers of leukocyte trafficking to areas of tissue injury in all tissues and organs.[19] Regardless of the target tissue, immune cell recruitment follows a universal cascade, which is primed by transient interactions between circulating leukocytes and vascular ECs.[20] Activation of vascular ECs by inflammatory cytokines is the first step of inflammatory response to tissue injury. This is owing to the expression of selectins and adhesion molecules on the surface of ECs, which ultimately leads to the recruitment of inflammatory cells to injured areas.[20–22] Although cytokines can only act on cells that express the respective cytokine receptors in sufficient amounts to activate signaling cascades in the cells and thus to activate a biological response, how cytokine receptor expression is actually regulated has been rarely addressed in the literature. Whether ADAR2 is involved in immune cell trafficking remains unknown.

Herein, we report that ADAR2 controls endothelial IL-6 signaling (IL-6 *trans*-signaling) and recruitment of circulating immune cells to vascular endothelium. We employed three mouse genetic models (global and vascular EC-restricted ADAR2 and IL6ST loss), four experimental disease models (sterile peritonitis, intravital microscopy of cremaster muscle microcirculation, hindlimb ischemia model, ischemic heart disease model), and three human cohort studies, including two independent cohorts of heart biopsies from either fatal acute or chronic ischemic heart disease (cIHD). Our findings reveal a role for ADAR2 in IL-6 cytokine receptor and immune cell trafficking under ischemic stress conditions, which is of utmost importance for EC-enriched muscle tissues whereby IL-6 signaling is induced.

RESULTS

Endothelial ADAR2 controls IL-6 *trans*-signaling

In order to investigate whether ADAR2 plays a role in EC function, we efficiently silenced ADAR2 in human primary vascular ECs (human umbilical vein ECs; HUVECs) (Figure S1A) followed by bulk RNA sequencing,[18] gene ontology analysis, and an Ingenuity pathway analysis (IPA). Comparison of the ADAR2-depleted EC transcriptome to scrambled control indicated that ADAR2 may regulate endothelial inflammatory response (Figure 1A) and especially interleukin-6 (IL-6) signaling (Figure S1B). Gp130 (encoded by *IL6ST*), a subunit of the IL-6 receptor, stood out among the genes related to significantly deregulated biological pathways, identified by GO analysis (Figure 1A; red bars) and IPA (Figure S1B). Silencing of endothelial ADAR2 in human ECs and in mouse lung ECs derived from *Adarb1*$^{-/-}$/*KI* mice reduced expression of gp130 by more than 50% (Figures 1B–1D, S1C,

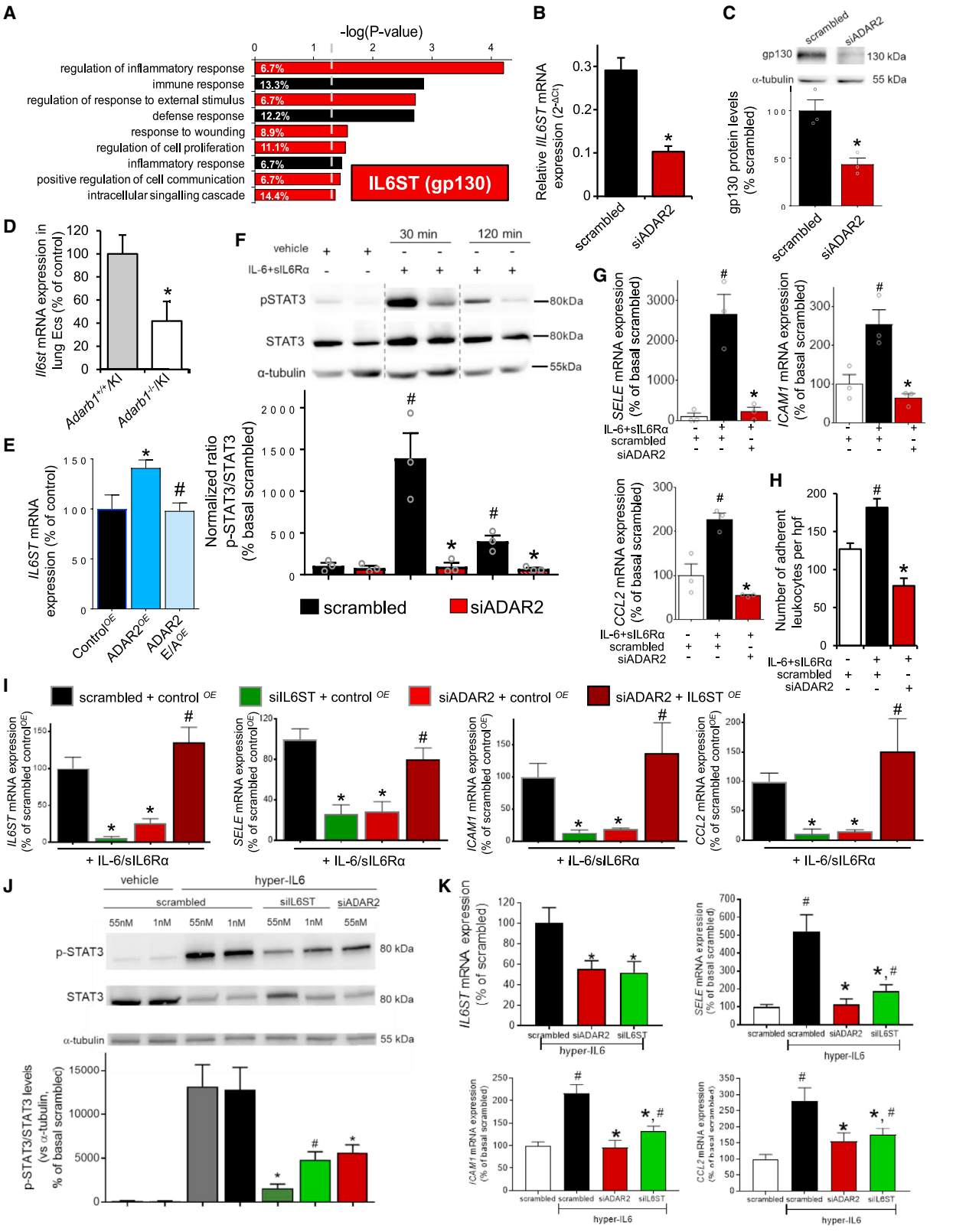

Figure 1. ADAR2 controls IL-6 *trans*-signaling cascade by regulating IL6ST expression in vascular endothelium

(A–K) Human umbilical vein endothelial cells (HUVECs) were transfected with scrambled nucleotides or with siRNA targeting ADAR2 (siADAR2) for 72 h, where indicated (A) gene ontology analysis of the ADAR2 regulated genes (n = 2 per condition; see also STAR Methods for details). The bar graph depicts −log(p value).

(legend continued on next page)

and S1D), while overexpression of ADAR2 exerted the opposite effects in human ECs (Figure 1E). In contrast, overexpression of an RNA-editing-deficient ADAR2 mutant (Figure 1E) or efficient silencing of ADAR1 had no influence on *IL6ST* mRNA expression in human ECs (Figure S1E).

Vascular ECs do not express the crucial subunit of the IL-6 receptor, the IL-6 receptor alpha (IL-6Rα), in sufficient protein levels for the induction of the canonical IL-6 signaling pathway[23] (Figure S1F), and hence, they have to rely on "*trans*-signaling" via gp130 to transduce IL-6 signals. This mechanism requires complexation of IL-6 with the soluble form of IL-6Rα (sIL-6Rα), which is secreted by neighboring cells.[23–26] As such, the induction of IL-6 *trans*-signaling-induced EC innate immune response is achieved with a combinational treatment of IL-6 and sIL-6Rα or simply with a unimolecular IL-6-sIL-6Rα (soluble IL-6Rα) chimeric protein[27] (namely hyper-IL-6, which simulates the physiological stimuli of the IL-6 *trans*-signaling). Indeed, comparative stimulation experiments with hyper-IL-6 and IL-6 alone verified the superior effect of IL-6 *trans*-signaling compared with the canonical IL-6 pathway for the induction of EC innate immune response (Figure S1F), as previously described for ECs[23,24,28] and other cells.[29]

Considering that gp130 interacts with other co-receptors that transmit signal for IL-6-like cytokines, we tested the presence of these co-receptors and the effect of ADAR2 in IL-6-like cytokine-signaling in ECs. In contrast to gp130, the rest IL-6-like cytokine receptors are barely expressed on the surface of ECs while ciliary neurotrophic factor receptor (CNTFR) expression could not be detected (Figure S1G). Among the rest gp130-dependent cytokines (ligands), oncostatin M was the only one to induce at least a modest pro-inflammatory response in ECs (Figure S1H). The mild effects of ADAR2 in oncostatin M-signaling may be based on the fact that oncostatin M utilizes one unit of gp130 while IL-6-IL-6Rα complex requires two units of gp130 to transmit their signals in vascular ECs (reviewed in Rose-John[30]). Taking into account that IL-6 is integral for endothelial inflammatory response[23,31] and gp130 is highly expressed in ECs, we henceforward focused on exploring the effect of ADAR2-mediated regulation of gp130 in IL-6 *trans*-signaling. In response to IL-6, intracellular STAT3 transiently interacts with gp130 and, upon phosphorylation, STAT3 translocates to the nucleus and gives rise to IL-6 *trans*-signaling-associated transcriptional products in ECs.[26] Indeed, silencing of ADAR2 severely reduced IL-6 *trans*-signaling, as evidenced by: (1) more than 3-fold decreased STAT3 phosphorylation levels, (2) severely defective expression of downstream adhesion genes including E-selectin (SELE), intercellular cell adhesion molecule-1 (ICAM-1), vascular cell adhesion molecule-1 (VCAM-1), and monocyte chemoattractant protein-1 (MCP-1; encoded by *CCL2* gene), (3) selective reduction in the secretion of IL-6 *trans*-signaling-induced secreted chemokines, MCP-1 and CXCL1, and (4) decreased leukocyte adhesion onto a monolayer of ECs *in vitro* (Figures 1F–1H and S1I–S1K). IPA analysis underscored these findings (Figure S1L). Overexpression of *IL6ST* restored the *SELE*, *ICAM1*, and *CCL2* mRNA expression after silencing of ADAR2 in ECs (Figure 1I). To corroborate these findings, gp130 was silenced in ECs proportionally to the mRNA and protein levels achieved by the silencing of ADAR2 (Figures S1M and S1N). A 55 % reduction of gp130 protein and mRNA expression drastically reduced the IL-6 *trans*-signaling cascade to comparable levels with the ones induced by the silencing of ADAR2 (Figures 1J and 1K), indicating that a 50% reduction of gp130 is sufficient to phenocopy the effects of ADAR2 silencing on IL-6 *trans*-signaling *in vitro*.

Together our data show that ADAR2 emerges as a potent modulator of gp130-dependent IL-6 *trans*-signaling in vascular endothelium.

ADAR2 is integral for IL-6 *trans*-signaling-driven immune cell trafficking

Considering that ADAR2 controls IL-6 *trans*-signaling-mediated EC responses and especially the expression of the adhesion mediators, SELE and ICAM-1 (Figure 1G), we hypothesized that ADAR2 may regulate the rolling and firm adhesion of immune cells to vascular endothelium. We used *Adarb1*$^{-/-}$/*Gria2* $^{R/R}$ mice that carry the edited (mutant) version of *GluR*, which rescues the early post-natal death of *Adarb1*$^{-/-}$ mice.[3] For simplicity reasons, henceforward, we will refer to this strain as *Adarb1*$^{-/-}$/KI. Using intravital imaging, we studied the effect of ADAR2 on IL-6-*trans*-signaling-mediated upregulation of adhesion molecules as well as the concomitant myeloid cell rolling and firm adhesion onto vascular endothelium of the cremasteric venule microcirculation in *Adarb1*$^{-/-}$/KI and respective control mice (Figures 2A and S2A–S2C). These experiments

The significance threshold is 1.3 for a p value of 0.05 and is denoted by a dashed gray line. Red bars indicate the terms containing interleukin 6 signal transducer (IL6ST; glycoprotein 130; gp130). The term enrichment percentage as calculated by the database is shown inside each bar.
(B and C) *IL6ST* mRNA levels (n = 5) (B) and gp130 protein levels (n = 3) (C).
(D) *Il6st* mRNA levels in murine primary endothelial cells (n = 4).
(E) *IL6ST* mRNA expression levels following ADAR2 overexpression (n = 4).
(F) Western blot of phosphorylated (p-STAT3) and total STAT3 protein levels and α-tubulin (n = 3). The excision sites of the lanes are indicated in gray dashed line. The bar graph shows the normalized intensity ratio p-STAT3/total STAT3 to α-tubulin.
(G) E-selectin (SELE; left), intercellular adhesion molecule-1 (ICAM1; right), and monocyte chemoattractant protein-1 (CCL2; bottom) mRNA expression after ADAR2 knockdown with or without IL-6/IL-6Rα-induced stimulation of HUVECs for 6 h (n = 3).
(H) Human leukocyte adhesion over HUVECs (n = 4).
(I) Rescue studies of E-selectin (SELE), ICAM-1 and CCL2 expression in the IL-6/IL-6Rα-stimulated HUVECs (4 h) after ADAR2 or IL6ST knockdown and overexpression of IL6ST (*Il6st*^{OE}) or control vector (*control*^{OE}) (n = 4).
(J) Western blot analysis (top) showing the levels of p-STAT3 in the phenocopy experiments (see also Figures S1M and S1N; n = 4).
(K) *IL6ST* mRNA and IL-6 *trans*-signaling cascade molecule mRNA expression in the phenocopy experiments (n = 5).
Data are presented as mean ± SEM for n independent biological replicates. Experimental groups were compared using a two-tailed Mann-Whitney U test or t test depending on data distribution for pairwise comparisons. *p < 0.05 versus scrambled control of the same time point or scrambled control; $^{\#}$p < 0.05 versus basal scrambled control. Bonferroni's multiple comparison test was used for comparing more than two groups.
See also Figures S1A–S1N.

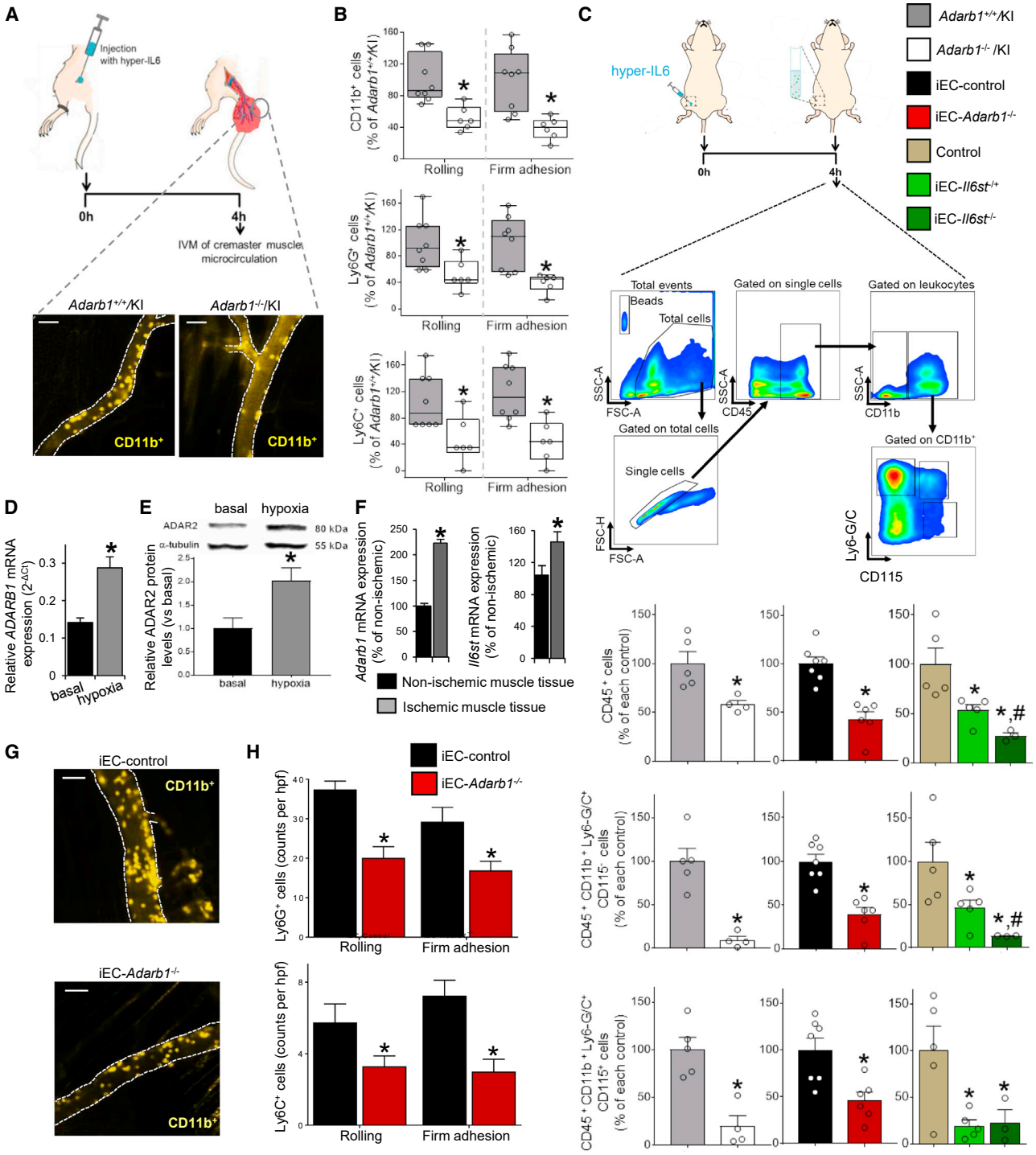

Figure 2. Endothelial ADAR2 controls immune cell trafficking in sterile inflammation

(A) Representative acquisition images from intravital microscopy depicting the antibody-tagged CD11b$^+$ (myeloid marker, yellow) cells in a post-capillary venule of the cremaster muscle of Adarb1$^{+/+}$/KI (n = 8; left) and *Adarb1*$^{-/-}$/KI (n = 6; right) mice. Scale bar represents 50 μm. See also STAR Methods and Video S1.

(B) Quantification of rolling and adhesion of CD11b$^+$ cells (top), Ly6G$^+$ cells (neutrophils; middle), and Ly6C$^+$ cells (classical monocytes; bottom).

(C) Adarb1$^{+/+}$/KI (n = 5; gray bar) and *Adarb1*$^{-/-}$/KI (n = 4; white bar) as well as inducible endothelial cell (iEC) restricted control (iEC-control; *Adarb1*$^{flox/flox}$/*Cdh5*-Cre$^{ERT2\ 0/0}$; n = 7; black bar) and *Adarb1*$^{-/-}$ (iEC-*Adarb1*$^{-/-}$; *Adarb1*$^{flox/flox}$/*Cdh5*-Cre$^{ERT2\ tg/0}$; n = 7; red bar) or control (*Il6st*$^{flox/flox}$/*Cdh5*-Cre$^{ERT2\ 0/0}$; n = 5; khaki bar) and iEC-Il6st$^{-/+}$ (*Il6st*$^{wt/flox}$/*Cdh5*-Cre$^{ERT2\ tg/0}$; n = 5; light green bar) or iEC-*Il6st*$^{-/-}$ (*Il6st*$^{flox/flox}$/*Cdh5*-Cre$^{ERT2\ tg/0}$; n = 3; dark green bar) mice were challenged with hyper-IL-6 and the peritoneal content was examined by flow cytometry with respect to the relative number of CD45$^+$ cells (leukocytes; C, top), CD11b$^+$Ly6-G/C$^+$ CD115$^-$ cells (neutrophils; C, middle), and CD11b$^+$Ly6-G/C$^+$ CD115$^+$ cells (classical monocytes; C, bottom).

(D and E) ADAR2 (*ADARB1*) expression in mRNA (D) and protein level (E) in hypoxic HUVECs (n = 5).

(legend continued on next page)

demonstrated a dampened rolling and adhesion of CD11b$^+$ (myeloid cells), Ly6G$^+$ (neutrophils), and Ly6C$^+$ (classical monocytes) cells over the hyper-IL-6-inflamed vascular endothelium of *Adarb1*$^{-/-}$/KI compared with littermate control mice (Figure 2B; Video S1). Consistent with the defective immune cell trafficking, downregulated expression of adhesion molecules was recorded in IL-6 *trans*-signaling-stimulated primary ECs isolated from these mice (Figure S2D).

Next, we measured the number of infiltrated leukocytes in peritoneal lavage after injecting hyper-IL-6 in global (*Adarb1*/KI) and endothelial-restricted ADAR2 knockout (*Adarb1*$^{-/-}$/*Cdh5*-CreERT2) mice (Figure S2E) as well as in endothelial-restricted IL6ST hemizygous (Il6st$^{-/+}$/*Cdh5*-CreERT2) and homozygous knockout (Il6st$^{-/-}$/*Cdh5*-CreERT2) mice generated by utilizing the inducible, vascular endothelial-promoter driven Cre recombinase strain (VE-cadherin(PAC)-Cre-ERT2 mice) (Figure 2C). The inducible vascular endothelial-restricted *Adarb1*$^{-/-}$ and IL6ST hemizygous and homozygous knockout mice will be referred in this manuscript as inducible endothelial cell (iEC)-*Adarb1*$^{-/-}$, iEC-Il6st$^{-/+}$, and iEC-Il6st$^{-/-}$, respectively. Flow cytometry analysis of the peritoneal lavage content revealed a profound reduction of leukocytes (CD45$^+$ cells), and specifically of neutrophils (Ly6-G/C$^+$ CD115$^-$ cells) and monocytes (Ly6-G/C$^+$ CD115$^+$ cells) in all the three strains compared with their corresponding controls (Figure 2C; white vs. gray, red vs. black, light green vs. khaki bars). Leukocyte subtype analysis revealed a $\geq$50% decrease in the infiltration of neutrophils and monocytes in iEC-*Adarb1*$^{-/-}$ and iEC-Il6st$^{-/+}$ mice (Figure 2C; white vs. red vs. light green bars). Complete knockout of gp130 almost abolished immune cell trafficking as evidenced in iEC-Il6st$^{-/-}$ mice (Figure 2C; khaki vs. dark green bars). Collectively, we show that endothelial ADAR2-IL6ST axis is indispensable for IL-6 *trans*-signaling-mediated immune cell trafficking *in vivo*.

ADAR2 is dispensable for immune and vascular system homeostasis

In order to investigate whether hematopoiesis/differentiation is compromised in response to ADAR2 absence which could explain the defective immune cell trafficking, we performed extensive immunophenotyping in *Adarb1*$^{-/-}$/KI or iEC-*Adarb1*$^{-/-}$ mice. Our findings showed that the abundance of the distinct immune cell subpopulations remained unaffected (Figures S3A–S3M), suggesting that, unlike ADAR1,[1,2,16] ADAR2 is dispensable for immune system development. This finding is concordant to the much higher expression of ADAR2 in ECs compared with hematopoietic cells, the unchanged immune cell counts in blood and bone marrow of the hyper-IL-6 stressed mice and in the peritoneal lavage in absence of hyper-IL-6 challenge between iEC-*Adarb1*$^{-/-}$ and control mice (Figures S4A–S4D). No deficiency was detected neither in the post-natal retinal vascular growth nor in the vascular branching of *Adarb1*$^{-/-}$/KI mice (Figure S4E), indicating that ADAR2 is similarly redundant for vascular growth.

Endothelial ADAR2 is required for ischemia-induced immune cell trafficking

IL-6 has been previously shown to be increased during ischemia, thereby triggering innate immune responses (reviewed in Epelman et al.[32]). ADAR2 is the only A-to-I RNA-editing enzyme increased by hypoxia in human ECs and is upregulated during ischemia in EC-enriched murine muscle tissues (Figures 2D–2F and S4F) which is in accordance to a previous report.[33]

By *in vivo* and *ex vivo* staining of post-capillary vessels of mice prior subjected to ischemic cremaster muscle injury, a 1.7-, 2-, and 4- fold increase was documented in the mean fluorescence intensity of ICAM-1, VCAM-1, and SELE, respectively, compared with sham-operated mice (Figure S4G). Selective blockade of IL-6 *trans*-signaling, using a chimeric protein of soluble gp130 (sgp130) which is the natural inhibitor of IL-6 *trans*-signaling,[34] impaired both the IL-6 *trans*-signaling-induced adhesion molecule expression and leukocyte adhesion in vessels of ischemic mice compared with control-treated animals (Figures S4H and S4I). Given the importance of IL-6 *trans*-signaling in ischemia-induced immune cell recruitment to vascular endothelium, intravital imaging of the ischemic cremaster muscle microcirculation revealed a substantial impairment of both rolling and firm adhesion of neutrophils and monocytes to the ADAR2-deficient endothelium (Figures 2G and 2H; Video S2). Consistent with these observations, the mean fluorescent signal intensity of the staining against the IL-6 *trans*-signaling-induced adhesion molecules was reduced in the ADAR2-deficient post-capillary vessels of ischemic mice compared with control vessels (Figure S4J).

We next sought to assess the relevance of our findings in a chronic ischemic muscle injury after permanent ligation of the femoral artery, marked by increased serum IL-6 concentration (Figures 3A and S5A). Immunohistological analysis of the post-capillaries of the adductor muscle, proximal to the site of injury, showed an upregulation of IL-6 *trans*-signaling-related inflammatory molecules, SELE, VCAM-1, ICAM-1, and MCP-1, protein in the ischemic limb compared with the non-ischemic limb of the iEC-control mice (Figures S5B–S5E). This notable increase was restored back to the non-ischemic levels in nearly all adhesion

(F) *Adarb1* (left) and *Il6st* (right) mRNA expression in murine non-ischemic (black bars) and ischemic (gray bars) skeletal muscle tissue lysates (n = 4 mice preparations).

(G and H) Representative acquisition images depict the antibody-tagged CD11b$^+$ (myeloid marker, yellow) cells in a post-capillary venule of the cremaster muscle of the iEC-control (*Adarb1*$^{flox/flox}$/*Cdh5*-Cre$^{ERT2\ 0/0}$; n = 7) and iEC-*Adarb1*$^{-/-}$ mice (n = 7). Scale bar represents 50 μm. See also Video S2. (H) Quantification of rolling and adhesion of Ly6G$^+$ cells (neutrophils) and Ly6C$^+$ cells (classical monocytes) was performed by counting the positive cells in at least two high power fields (hpf) per mouse.

The boxplots (B) for n animals per group indicate from top to bottom: maximum, third quartile, median, first quartile and minimum. The percentage (%) of the mean value of each control group values is shown. The bar graphs (C–F and H) for n mice or n independent biological replicates indicate the mean ± SEM. Measurements performed in at least two hpf unless otherwise stated (H). Experimental groups were compared using a two-tailed Mann-Whitney U test or unpaired t test depending on data distribution. Each *in vivo* experimentation was performed once by testing simultaneously n animals per group. *p < 0.05; versus control/iEC-control or basal/non-ischemic and $^{\#}$p < 0.05; versus iEC-Il6st$^{-/+}$.

See also Figures S2A–S2E, S3A–S3M, and S4A–S4J and Videos S1 and S2.

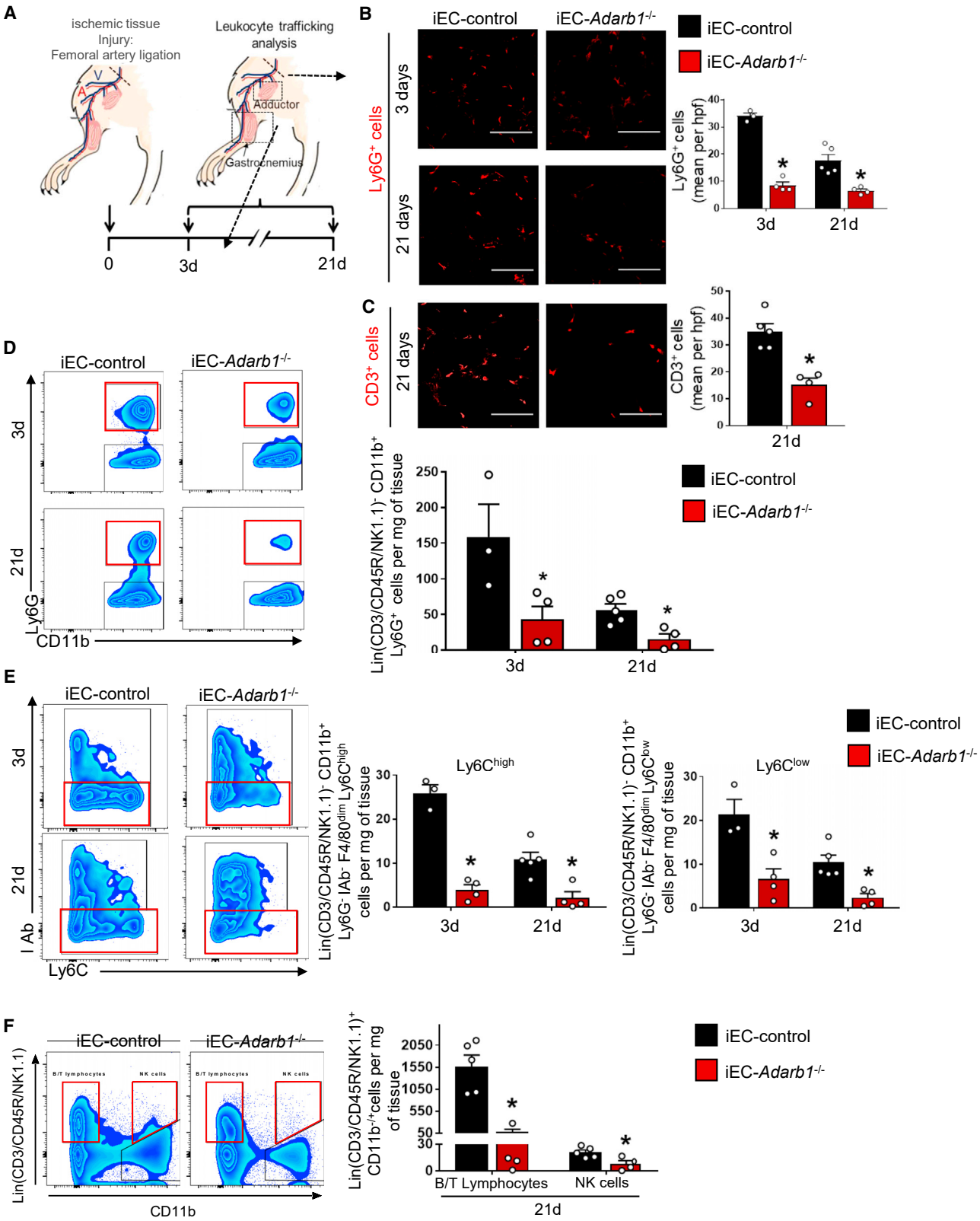

Figure 3. Endothelial ADAR2 is required for immune cell infiltration in ischemic muscle disease

(A–F) The femoral artery of the inducible endothelial cell (iEC) restricted *Adarb1*$^{-/-}$ (iEC-*Adarb1*$^{-/-}$, *Adarb1*$^{flox/flox}$/*Cdh5*-Cre$^{ERT2\ tg/0}$, n = 4) and iEC-control (Adarb1$^{+/+}$/*Cdh5*-Cre$^{ERT2\ tg/0}$, n = 3 for the 3 days post-injury studies and n = 5 for the 21 days post-injury studies) mice was ligated and 3 or 21 days later the

(legend continued on next page)

molecules apart from ICAM-1 akin probably to its high baseline protein levels (Figures S5B–S5E). Immunohistological analysis of adductor muscle revealed a dampened infiltration of neutrophils by 3- to 5-fold in both early (3 days) and late (21 days) stages after hindlimb ischemia injury in EC-ADAR2-deficient mice compared with controls, respectively (Figure 3B). Similarly, infiltrating $CD3^+$ T cells were also 2-fold decreased in the injured muscle of iEC-*Adarb1*$^{-/-}$ mice (Figure 3C). Flow cytometry analysis of the gastrocnemius muscle confirmed the immunostaining results while additionally revealing a reduction in the number of neutrophils as well as of $Ly6C^{high}$ and $Ly6C^{low}$ monocytes at both time points (Figures 3D, 3E, and S5F). Lymphocytes including natural killer (NK) cells play an important role in the late phases of tissue healing post ischemic injury.[35] Flow cytometric analysis 21 days post hindlimb ischemia injury revealed a 3-fold decrease of infiltrating lymphocytes including NK cells in the EC-ADAR2-knockout mice (Figure 3F).

In conclusion, EC ADAR2 is imperative for acute and chronic ischemia-induced immune cell trafficking by controlling immune cell rolling and firm adhesion onto vascular endothelium.

Relevance of endothelial ADAR2 expression for immune cell trafficking in human acute and chronic ischemic heart diseases

In view of the findings in the experimental mouse models, we next evaluated the relevance of our findings for human pathology. We examined three cohorts of patients with either acute or cIHD, the major cause of death worldwide. Serum IL-6 concentration was found to be rapidly increased by 3.5-fold in patients within the first 24 h after acute myocardial infarction (AMI), which is caused by acute thrombotic occlusion of an epicardial coronary artery and was associated with the extent of ischemic time (Figures 4A and 4B; Tables S1 and S2). Patients at the highest tertile of IL-6 increase exhibited 4-fold higher concentration of the cardiac injury marker, troponin T, upon admission to the hospital, and CMR-detected microvascular obstruction compared with those at the lowest tertile (Figures 4C and 4D). A higher IL-6 increase over the first 24 h post AMI was a reliable predictor for larger infarct size and reduced LVEF (Figures 4E and 4F). Despite the very high baseline concentration at the time of patient admission to the hospital due to ST-segment elevation myocardial infarction (STEMI) (baseline sIL-6Rα: mean ± SEM: 43.6 ± 2 ng/mL), the circulating concentration of IL-6Rα protein was also slightly but significantly increased in these patients compared with baseline measurements (Figure S6A). Post-mortem histological examination revealed a profound increase of ADAR2 expression in ECs in ischemic heart tissues compared with healthy heart tissues derived from individuals who passed away due non-cardiac causes (Figures 4G and 4H). Staining of these tissues revealed a strong positive association ($r = 0.86$, $p < 0.0001$) between EC ADAR2 and the number of infiltrated perivascular leukocyte in the ischemic heart tissues (Figures 4G and 4I).

We also studied the presence and extent of IL-6 signaling and ADAR2 association with infiltrated leukocytes in patients with cIHD (Tables S3 and S4). We observed an 8-fold increase of IL-6 concentration in serum (Figure 5A, left) and a 5-fold increase of the mean fluorescent signal of IL-6 protein (Figure 5A, right) accompanied by 4-fold augmented pSTAT3 presence (Figure 5B) in cardiac tissues of cIHD patients compared with control individuals or control healthy heart tissue. *ADARB1* and *IL6ST* mRNA expression was also increased in cIHD heart tissues (Figure 5C). The mRNA expression of the IL-6 co-receptor, *IL6ST*, was also strongly associated with the extent of *ADARB1* expression ($r = 0.73$, $p < 0.0001$; Figure 5D) in heart tissues. Both *IL6ST* and *ADARB1* mRNA expression were associated with immediate downstream signaling of IL-6 and STAT3 phosphorylation (Figure 5E). Similar to IL-6, cardiac protein levels of IL-6Rα in cardiac lysates were also increased in these patients (Figure 5F). Histological evaluation of heart tissues derived from cIHD patients or controls confirmed the distinct increase of ADAR2 and IL6ST in vascular ECs (Figures 5G–5I). Increased numbers of vascular EC expressing ADAR2 were associated with a higher perivascular leukocyte infiltration (Figures 5I and 5J).

In order to corroborate the human findings, we investigated the causal relationship of ADAR2-IL6ST regulatory axis on immune cell trafficking in a murine model of cIHD (Figure S6B). The variable effect of permanent left anterior descending (LAD) ligation in the development of ischemic heart disease was monitored by small animal CMR imaging (Figures S6C–S6E). Mice with severe MI exhibited 6-fold increased concentration of circulating IL-6 compared with mice undergoing mild injury (Figure S6F). *ADARB1* mRNA expression was increased by 3-fold in mice subjected to severe MI compared with those subjected to mild AMI and was strongly associated with the expression of *IL6ST* ($n = 8$, $r = 0.953$, $p < 0.001$; Figure S6G). Genetic ablation of ADAR2 in mice presented with a 3-fold decreased *Il6st* expression in heart tissues 4 weeks post myocardial infarction (Figure S6H). Similar to the chronic hindlimb ischemia model findings in EC-restricted ADAR2 knockout mice (Figure 3), a significant reduction in $CD45^+$ cell infiltration in ADAR2-deficient mice following a severe AMI along with a profoundly decreased scar size in ADAR2-deficient mice reminiscent of the clinical finding (Figure 4E) was observed (Figures S6I and S6J). IL-6 *trans*-signaling-induced adhesion molecules expression in the vessels of these animals was also reduced compared with the control tissues (Figure S6K).

adductor (proximate to the ligation site) as well as the gastrocnemius (distal to the ligation site) muscle were analyzed (A). Representative images from the immunohistochemistry of $Ly6G^+$ cells (neutrophils; present at 3 and 21 days post-ischemia) (B) and $CD3^+$ cells (lymphocytes; present at 21 days post-ischemia) (C) and quantification bar graphs. The quantification of the immunohistochemistry images (B and C) was performed by calculating the median of the counts of 4 random high power fields (hpf) per mouse. Scale bars represent the mean ± SEM as calculated per experimental group. Scale bars, 100 μm. Flow cytometry zebra plots of individual mice showing the gated populations and the quantification bar graphs of $Lin(CD3/CD45R/NK1.1)^-$ $CD11b^+$ $Ly6G^+$ (neutrophils) (D), $Lin(CD3/CD45R/NK1.1)^+CD11b^-$ (B/T lymphocytes)/$CD11b^+$ (NK cells) (E), $Lin(CD3/CD45R/NK1.1)^-$ $CD11b^+$ $Ly6G^-$ IAb^- $F4/80^{dim}$ $Ly6C^{high}$ (classical monocytes)/$Ly6C^{low}$ (non-classical monocytes) (F) cells. For the full gating strategy see also Figure S5F.

The bar graphs (D–F) for n number of mice tested indicate the mean ± SEM, unless otherwise stated. Measurements were performed as one replicate unless otherwise stated. Experimental groups were compared using a two-tailed Mann-Whitney U test. *$p < 0.05$; versus iEC-control.

See also Figures S5A–S5F.

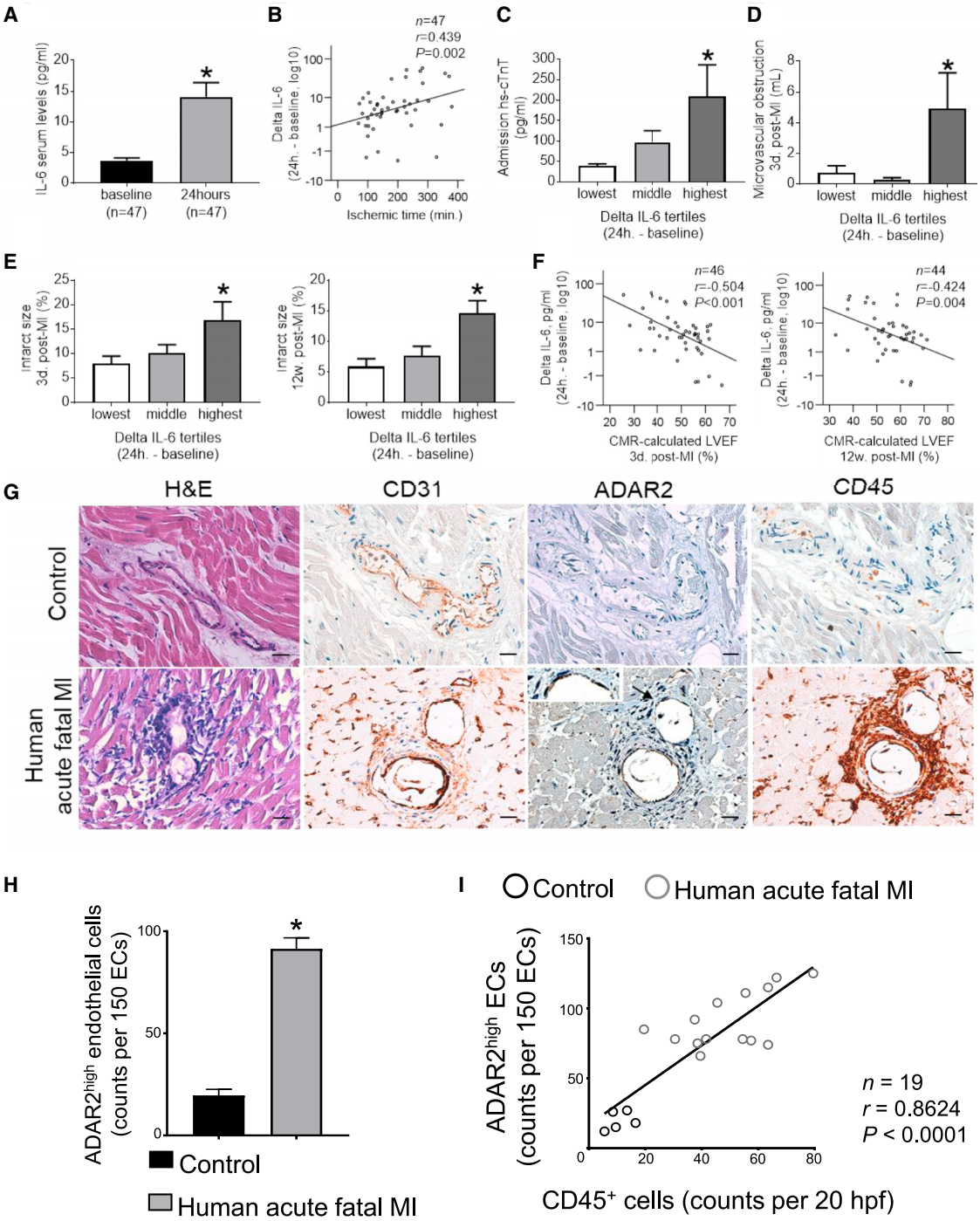

Figure 4. Endothelial ADAR2 is associated with perivascular immune cell infiltration in acute myocardial infarction

(A) IL-6 serum concentrations (IL-6 levels) were determined in 47 patients undergoing primary percutaneous coronary intervention (PPCI) for acute myocardial infarction (AMI) at baseline and 24 h after reperfusion of the occluded vessel.

(B) Correlation graph of ischemic time (min) with the change in IL-6 serum concentration over time (Delta IL-6; IL-6 24 h minus baseline).

(C–E) Patients were classified in tertiles according to change of IL-6 circulating concentration levels over time (Delta IL-6 tertiles). Bar graphs depict levels of admission high-sensitivity cardiac troponin T (C), volume of microvascular obstruction (mL, D), and infarct size as percentage of the left ventricle determined by cardiac magnetic resonance (CMR) imaging 3 days (E, left) and 12 weeks (E, right) post-MI in tertiles of Delta IL-6.

(F) Correlation graphs of left ventricular ejection fraction (LVEF) with Delta IL-6 3 days (left) and 12 weeks (right) post-MI determined by CMR.

(G) Representative images from histological analysis of serial sections of autopsy human myocardial tissue from subjects who suffered an acute fatal myocardial infarction (MI) (bottom, n = 14) and control non-infarcted heart tissues (top, n = 5) stained with H&E (left), CD31 (brown, endothelial cell marker) (middle left) and

(legend continued on next page)

Collectively, these findings reveal the pathophysiologic relevance of ADAR2 for IL-6 signaling and immune cell trafficking in human ischemic heart diseases.

ADAR2 controls the expression of a group of miRNAs tasked with targeting the *IL6ST* 3′ UTR

We sought to increase our understanding of the potential mechanism underlying the ADAR2-mediated regulation of IL6ST. Since silencing of ADAR2 prominently reduced *IL6ST* mRNA stability (Figure 6A), which was further confirmed by an *IL6ST* 3′ UTR luciferase reporter assay (Figure 6B), we reasoned that the regulation of *IL6ST* expression by ADAR2 occurs at the post-transcriptional level. Nevertheless, no RNA-editing events were observed on the *IL6ST* transcript in ECs.[18] Accordingly, we excluded a direct RNA editing effect of ADAR2 on *IL6ST* mRNA stability. ADARs may also affect RNA stability by interfering with the microRNA (miRNA; miR)-mediated post-transcriptional regulation of mRNAs.[11] Specifically, ADARs may edit certain miRNA precursors, affecting their function by either redirecting of these miRNAs to other target mRNAs[36,37] or by inhibiting or promoting the Dicer-dependent miRNA processing.[38–40] Hence, we examined whether ADAR2-mediated RNA editing may either retarget mature miRNAs to regulate *IL6ST* mRNA or regulate the abundance of mature miRNAs in ECs that target *IL6ST* mRNA. To assess this hypothesis, we performed a series of unbiased transcriptome-wide analyses. First, RNA-editing analysis of the seed regions of the mature miRNAs in ECs revealed only a handful of miRNAs that are edited in their seed region, but none of them is predicted to target *IL6ST* before or after RNA editing occurs (data not shown). miR-sequencing experiments upon silencing of ADAR2 reported an increased expression of several miRs. The majority of those deregulated miRs was predicted to target *IL6ST* mRNA (Figure 6C). Those miRs, which were found to be conserved among humans and mice as well as to be regulated by ADAR2, were further assessed by validation through TaqMan-based assays. A pronounced upregulation of two particular miRNAs, miR-199a-5p and miR-335-3p, in human and murine ECs upon silencing of ADAR2 (Figures 6D, 6E, and S7A) was noticed, hinting that these miRNAs may target the *IL6ST* transcript. Consistently, ADAR2 overexpression conferred the opposite effect on the mature miRNA expression (Figure 6F), while ADAR1 silencing exerted no effect (Figure S7B). Those two outstanding miRs were also found to be upregulated in the hearts of ADAR2-null mice (Figure S7C). Overexpression of these miRNAs resulted in decreased endothelial *IL6ST* mRNA expression (Figure 6G), as well as reduced luciferase activity of *IL6ST* 3′ UTR (Figure 6H). Conversely, inhibition of the miRNAs partially restored the *IL6ST* mRNA expression after silencing of ADAR2 (Figure 6I), thus substantiating the pivotal role of these two miRNAs for ADAR2-mediated regulation of gp130.

Inhibition of Drosha binding to a group of primary microRNAs by ADAR2-mediated adenosine-to-inosine RNA editing controls IL6ST expression

We next examined how ADAR2 may inhibit the expression of mature miR-199a-5p and miR-335-3p in ECs. After excluding a transcriptional regulation (Figure S7D) and taking into consideration the nuclear localization of ADAR2, we hypothesized that ADAR2 may control the maturation process of these miRNAs. ADAR2 edits several adenosine residues in their stem-loop by directly binding to pri-mir-199a-1, pri-mir-199a-2, and pri-mir-335 in human and murine ECs (Figures 7A–7C, S7E, and S7F). These editing sites (Figure 7C) are localized within a region covering approximately 20 nt upstream and 25 nt downstream of the Drosha cleavage sites and specifically in the immediate vicinity and/or inside the stem-loop, which has been previously reported to be adequate to ensure Drosha recognition, binding, and processing.[41] Therefore, we postulated that ADAR2 may control Drosha recruitment to these pri-miRNAs. Accordingly, pri-mir-199a-1, pri-mir-199a-2, and pri-mir-335 were 5- to 15-fold enriched in Drosha-precipitates of EC lysates after silencing of ADAR2 (Figure 7D), suggesting that ADAR2-catalyzed RNA editing of these specific pri-miRNAs profoundly inhibits Drosha-dependent miRNA processing. This finding was further supported by demonstrating that efficient silencing of Drosha upregulates the expression of gp130 while co-silencing of ADAR2 and Drosha in ECs elicited a complete rescue of the ADAR2 silencing-mediated effects on mature miRNA and *IL6ST* mRNA expression (Figures 7E–7G, S7G, and S7H).

To test, as a proof-of-concept, whether RNA editing may be a determinant for the expression of the two miRNAs and concomitant gp130 expression, we generated CMV-driven pri-miRNA wild-type and edited constructs by adapting a similar strategy that we and others have previously described for complexed, non-coding regions, including pri-miRNAs.[18,38] Accordingly, we generated four distinct constructs containing either pri-mir-199a1, which is the most edited among the two pri-miRNAs that give rise to mature miR-199a-5p, or pri-mir-335 that is processed into the mature miR-335-3p, with or without A-to-G mutations in order to mimic the edited and unedited (wild-type) version of these pri-miRNAs, respectively (Figure 7H). Overexpression of the edited version of either pri-mir-199a1 or pri-mir-335 in primary ECs resulted in 2.1- or 1.6-fold increased *IL6ST* mRNA expression compared with their wild-type forms, respectively (Figures 7I and 7J). Mechanistically, the edited forms of both pri-miRNAs were found to be much less potent

ADAR2 (brown; middle right), and CD45 (a pan-leukocyte marker, brown; right). The superimposed image represents a 400× magnification to enable the better visualization of the indicated (arrow) part of the vessel. Scale bars, 60 μm. The CD31, ADAR2, and CD45-stained tissues were counterstained with H&E.

(H) The bar graph shows the quantification of the ADAR2^{high}-expressing ECs per 150 counted vascular endothelial cells in high power field (hpf) within each tested tissue.

(I) Correlation graph of ADAR2^{high}-expressing ECs and CD45^{+} cells. The black and light gray circles denote the individual values of each control subject and patient with acute fatal MI, respectively.

Descriptive characteristics of the Newcastle cohort are available in Tables S1 and S2. The bar graphs (A, C, D, E, and H) for n individuals indicate the mean ± SEM. Experimental groups were compared using a two-tailed Mann-Whitney *U* test or independent samples t test depending on the data distribution. *$p < 0.05$ versus control, baseline, or lowest Delta IL-6 tertile. Correlation coefficient *r* and p value (B, F, and I) were calculated by the Pearson correlation coefficient test.

See also Figure S6A and Tables S1 and S2.

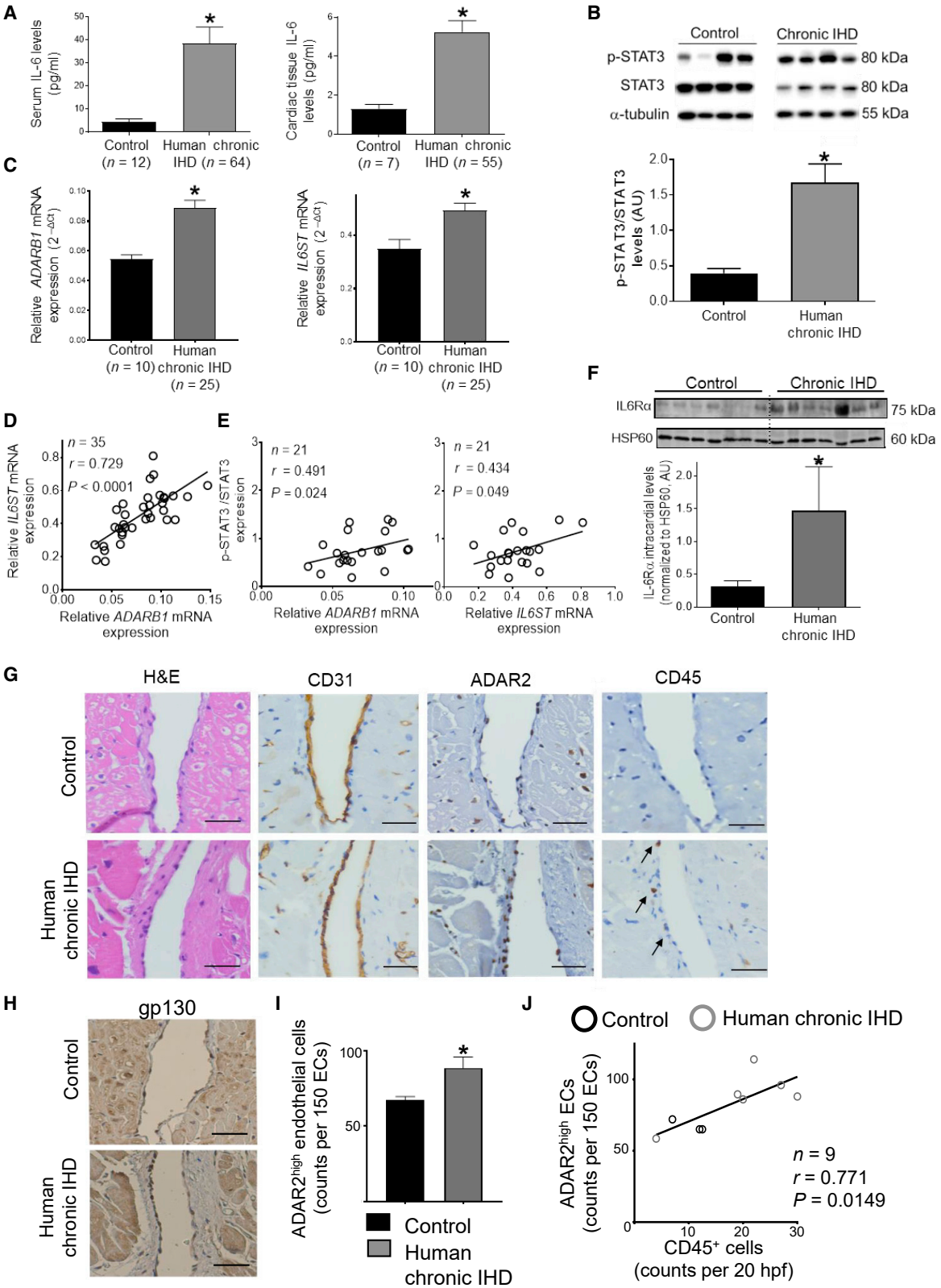

(legend on next page)

in respect to giving rise to their mature miRs compared with their wild-type versions (Figures 7K and 7L).

Conclusively, these results suggest that ADAR2-induced RNA editing of a specific group of primary miRNAs, including pri-mir-199a-1, pri-mir-199a-2, and pri-mir-335 studied here, disrupts Drosha binding and maturation of these miRNAs in ECs. In this way, endothelial ADAR2 promotes the expression of the gp130 and endothelial immune response to IL-6, an important biological process that controls immune cell trafficking in ischemic muscle diseases.

DISCUSSION

RNA modifications severely impact multiple facets of RNA metabolism with repercussions for gene expression and biological processes (recently reviewed in Gatsiou and Stellos[13]). Despite the recent flourishing of research on RNA modifications and the crucial roles that have been ascribed to mediate innate immune responses mainly by fine-tuning normal hematopoietic processes,[15,16] their potential involvement in immune cell trafficking remains elusive. We report an epitranscriptional mechanism orchestrating immune cell trafficking, a fundamental step of immune response. Endothelial ADAR2 regulates the concurrent transcription of several traffic mediators, including the adhesion molecules SELE, ICAM-1, and VCAM-1 and the chemokine MCP-1, which are all involved in several IL-6-related diseases. Therefore, future efforts are required to test whether therapeutic manipulation of ADAR2 efficiently inhibits IL-6 *trans*-signaling and excessive leukocyte infiltration in diseased tissues, thus counteracting (1) the lack of tissue specificity of anti-cytokine treatments, (2) the redundancy of the inflammatory mediators, and (3) the undesired side effects elicited by breaching the essential homeostatic role of IL-6/gp130 signaling.

We have previously demonstrated that ADAR1-induced RNA editing of primate-specific *Alu* elements leads to increased pro-inflammatory gene expression in human atherosclerosis[18,42] and several autoimmune diseases.[43,44] Although genetic deletion of ADAR1 leads to embryonic lethality as a result of the failure of normal homeostatic hematopoiesis and organ development,[16] genetic deletion of ADAR2 does not seem to affect development or non-neuronal tissue homeostasis. In this study, we delineated a stress-specific mechanism by which tissue specific-ADAR2 controls a vital step of innate immune response, the IL-6 *trans*-signaling-induced activation of ECs and subsequent immune cell trafficking, without compromising any immune or vascular system homeostatic processes.

Ischemic disease is the leading cause of death in the developed world. ECs are the first cells to sense the local hypoxic microenvironment and are therefore in a pole position to orchestrate the immune responses to ischemic injury.[45] We and others previously suggested that endothelial A-to-I RNA editing is induced by environmental stimuli including cytokines or hypoxia.[18,33] Here, we studied the effect of hypoxia in ADAR expression in ECs receiving pre-equilibrated hypoxic medium before the treatment commences. In contrast to the protein abundance of ADAR1 and ADAR3, which remained unchanged upon exposure of HUVECs to hypoxia, ADAR2 expression was found to be increased in hypoxic ECs, ischemic muscle tissues as well as in vascular ECs in heart biopsies derived from patients who underwent a fatal AMI or with a cIHD. This increase in ADAR2 expression was strongly associated with an elevation of gp130 expression, the IL-6 co-receptor in both cell culture experiments and murine and human ischemic heart tissues. Upon ischemia, IL-6 is increased in the blood leading to enhanced endothelial IL-6 signaling as evidenced by increased STAT3 phosphorylation. Using three ischemic injury disease models, we observed that ADAR2 ablation results in 50%–80% reduction in immune cell trafficking within ischemic muscle tissues. Collectively, considering the strong induction of IL-6, ADAR2, and IL6ST in ischemia, we conclude that ADAR2 is an important driver of immune cell recruitment to ischemic vascular endothelium.

This study adds another layer of control to the regulation of endothelial ischemic and IL-6 *trans*-signaling-induced inflammatory responses. We report that ADAR2-induced RNA editing of primary miRNAs inhibits their processing leading to decreased mature miRNA abundance and, subsequently, safeguarding gp130 expression and IL-6 *trans*-signaling cascade. We show that ADAR2-induced RNA editing of primary miRNAs directly interferes with Drosha binding in primary cells. Apart from

Figure 5. Endothelial ADAR2 is associated with IL-6 *trans*-signaling cascade in chronic ischemic heart disease

(A) IL-6 protein concentration levels measured in the serum (left) and tissue (right) of individuals with chronic ischemic heart disease (IHD) or without (control).

(B) Western blot analysis of phosphorylated STAT3 (pSTAT3) in control (n = 13) and chronic IHD individuals (n = 55) normalized to alpha-tubulin and STAT3 levels (arbitrary units, AUs).

(C) *ADARB1* (left) and *IL6ST* (right) mRNA expression in left ventricle biopsies from the total chronic IHD cohort (n = 25) and control individuals (n = 10).

(D) Scatterplot of *ADARB1* (*ADAR2*) with *IL6ST* mRNA expression in the human left ventricle chronic IHD cohort (total cohort; n = 35).

(E) Scatterplot of p-STAT3/STAT3 ratio with *ADARB1* (left panel) and *IL6ST* (right panel) mRNA expression in the human left ventricle chronic IHD subcohort in which these three parameters have been quantified in the same patients (n = 21 pairs for pSTAT3/STAT3 vs. *ADARB1* or *IL6ST*).

(F) Western blot analysis of IL-6Rα protein measured in heart tissue of individuals with chronic IHD (n = 7) or control (n = 7) normalized to HSP60 protein (arbitrary units, AUs).

(G and H) Representative images from a histologically analyzed subcohort of the total cohort of the human left ventricle biopsies from patients with chronic IHD (G, bottom, n = 6) and control subjects (G, top, n = 3, see also STAR Methods) stained with H&E (left), CD31 (brown, endothelial cell marker; G, middle left), ADAR2 (brown; middle right), and CD45 (brown, leukocyte marker; G, right) and gp130 (brown) (H). Scale bars, 50 μm. The CD31, ADAR2, and CD45-stained tissues were counterstained with H&E.

(I) The bar graph represents the quantification of the ADAR2^{high}-expressing ECs per 150 counted ECs in the tissues in hpf within each tissue.

(J) Scatterplot of ADAR2^{high}-expressing ECs and CD45^{+} cells. The black and dark gray circles represent the individual values of each control subject and patient with chronic IHD, respectively.

The bar graphs (A, B, C, F, and I) for n individuals or biological independent samples indicate the mean ± SEM. Experimental groups were compared using a two-tailed Mann-Whitney *U* test. *p < 0.05 versus control. Correlation coefficient *r* and p value (D, F, and J) were calculated by Pearson correlation coefficient test. See also Figures S6B–S6K and Tables S3 and S4.

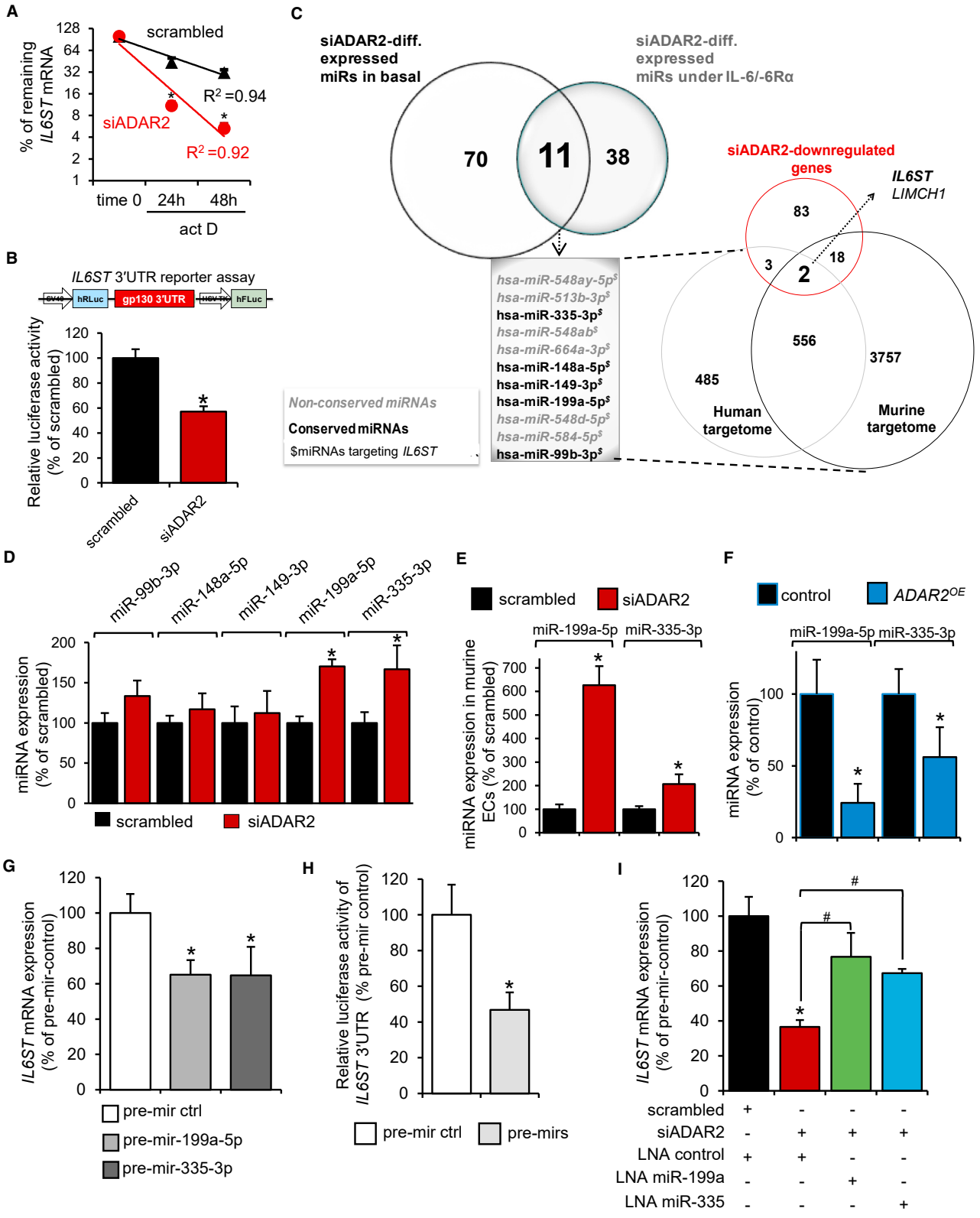

Figure 6. Endothelial ADAR2 inhibits the biogenesis of miRNAs that target *IL6ST* 3′ UTR

(A) Expression of *IL6ST* mRNA measured by real-time qPCR (n = 3) at the indicated time points after transcriptional inhibition of scrambled or ADAR2-silenced HUVECs with actinomycin D (act D).

(legend continued on next page)

ischemic diseases, our findings are of utmost importance to diseases that are linked with high IL-6 levels including autoimmune inflammatory diseases,[46] severe acute-pancreatitis-associated lung injury,[47] ileitis,[48] and cancer,[49] providing insights into the epitranscriptional mechanisms involved in the regulation of gene expression under stress conditions. Finally, this study may serve as a paradigm for delineating RNA-editing-based mechanisms in health and disease.

Limitations of the study

Our findings suggest that ADAR2-induced RNA editing enables IL-6 *trans*-signaling in ECs and, thus, immune cell trafficking. However, further cellular processes that relate to gp130-mediated signaling pathway (reviewed in Jones et al.[49] and Garbers et al.[50]) shall be investigated in light of this study. Mechanistically, we showed that primary miRNA editing overwrites the default transcriptional program by altering mRNA stability and, thus, gene expression. We believe the reason why relatively low editing levels of specific sites can effect functional changes is the high amount of editing sites within a single RNA molecule that are simultaneously being edited amplifying in this way the impact on gene expression. Once technological advances allow the characterization of specific nucleotides within individual RNA molecules (discussed in Gatsiou and Stellos[13]), future studies are warranted to infer a more detailed distribution of RNA edits per individual RNA molecule.

STAR★METHODS

Detailed methods are provided in the online version of this paper and include the following:

SUPPLEMENTAL INFORMATION

Supplemental information can be found online at https://doi.org/10.1016/j.immuni.2023.03.021.

ACKNOWLEDGMENTS

The study is supported by grants from the European Research Council (ERC) under the European Union's Horizon 2020 research and innovation programme (MODVASC, grant agreement no 759248), the German Research Foundation DFG (SFB834, project number 75732319 and SFB1366, project number 394046768), the Else Kröner-Fresenius-Stiftung and the DZHK to K. Stellos and from the UKRI BBSRC to A. Gatsiou and K. Stellos. O.S. is supported by DFG (SFB914/B08 and SFB1123 TP A6/B5). M.S. is supported by DFG (SFB914/B01 and TRR332/C02); O.S., M.S., and C.S.-R. by TRR332 TP A1, A2, C2, and Z1; S.G.D. by the AHA Heart Failure Strategically Focused Research Network grant 16SFRN29020000, NHLBI R01 grant HL135121-01, NHLBI R01 grant HL132067-01A1, the Nora Eccles Treadwell Foundation and the Merit Review Award I01 CX002291 U.S. Dept of Veteran Affairs; A. Gallo by AIRC IG no. 22080; A.W. and T.R. by the DFG grant SFB/TRR 355/1 (project number: 490846870); and C.T. by the German Research Foundation (DFG) CRC1382/403224013 and SFB TR285/10-2. The authors would like to express their gratitude to the independent expert pathologist Dr. Georgios Petrakis (Aristotle University of Thessaloniki) for assisting with histopathological assessment of the tissues as well as to Marco Sachse (Goethe University) and Maria Birgaoanu (Newcastle University) for help with cell culture/RNA preparations and murine pri-mir editing studies, respectively. Nikolaos Vlachogiannis (Newcastle University), Fortunata Tina Jung and Maria Polycarpou-Schwartz (Heidelberg University), and other former and current members of Stellos lab are thanked for providing technical support, proofreading of the manuscript, and helpful discussions. Marco Hagenmueller and Sumra Nazir (Heidelberg University) are thanked for assisting in a part of animal organ harvest. The Newcastle Bioinformatic Support Unit is thanked for helping with the IPA analysis. We thank Prof. Ralf Adams for providing the VE-Cadherin(PAC)-Cre-ERT2 mice.

(B) Relative luciferase activity of scrambled control- and siADAR2- transfected and *IL6ST* 3′ UTR-overexpressing HUVECs (n = 6).
(C) Venn diagrams of the differentially regulated miRNAs in the presence or absence of ADAR2 in unstimulated (basal) and IL-6/IL-6Rα-stimulated HUVECs. Non-conserved and conserved miRNAs are denoted in gray/italics font and bold, black font, respectively. MicroRNAs predicted to target *IL6ST* mRNA are indicated with "$".
(D) Human mature miRNA expression in scrambled control- and siADAR2- transfected HUVECs (n = 5).
(E) Expression of murine mature miR-199a-5p and miR-335-3p in scrambled control and siADAR2-transfected murine ECs (n = 4) confirming the upregulation of these miRNAs in murine ECs.
(F) miR-199a-5p and miR-335-3p expression after overexpression of ADAR2 in HUVECs (n = 4).
(G and H) HUVECs treated with precursors of miR-199a-5p (pre-mir-199a), miR-335-3p (pre-mir-335), both miRs (pre-mirs) or control (pre-mir ctrl) for 72 h, as indicated, were assessed for *IL6ST* mRNA expression levels (n = 4) (G) or the relative luciferase activity of the *IL6ST* 3′ UTR reporter (n = 6) (H).
(I) Rescue studies using HUVECs treated prior with LNA-based inhibitors of miR-199a-5p and miR-335-3p for 72 h. The *IL6ST* mRNA expression was measured by real-time qPCR (n = 4).
Data are presented as mean ± SEM for n biological independent replicates. Experimental groups were compared using a two-tailed Mann-Whitney *U* test. *p < 0.05; versus scrambled/control/pre-mir ctrl; or versus scrambled control after treatment with LNA control. #p < 0.05; versus siADAR2 after treatment with LNA control.
See also Figures S7A–S7D.

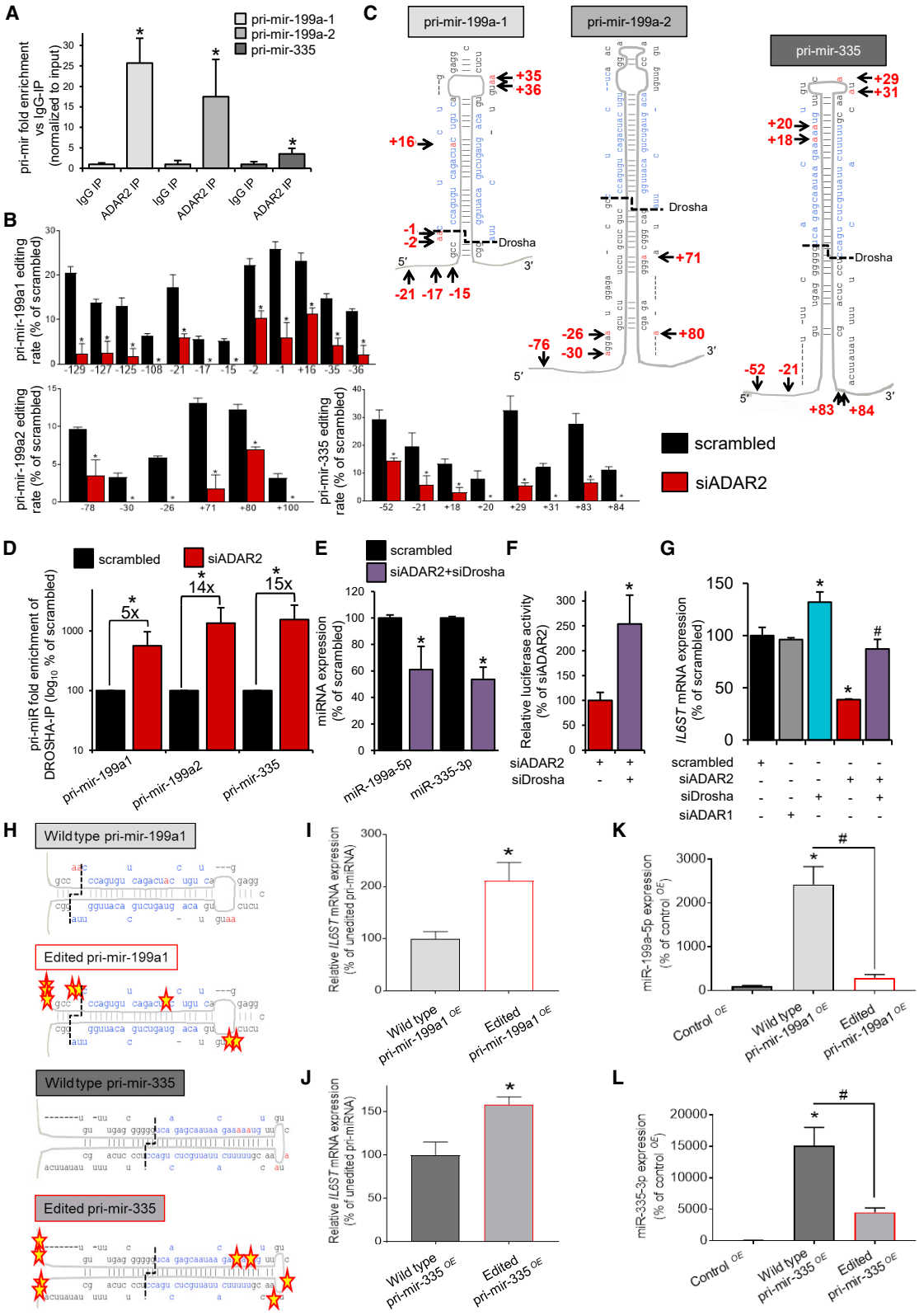

(legend on next page)

We are particularly grateful to Prof. Nikolaos G Frangogiannis (Albert Einstein College of Medicine) for critically reading the manuscript.

AUTHOR CONTRIBUTIONS

A. Gatsiou and K. Stellos conceptualized the study, designed and guided research, and analyzed and interpreted the experiments. A. Gatsiou drafted and K. Stellos edited the manuscript with input from all co-authors. A. Gatsiou performed the molecular biology experiments and part of the cell biology studies including the immune cell tissue characterization of the HLI model. S.T.-C. performed and analyzed the data of the hypoxia EC experiments, the murine MI and HLI adhesion molecule staining experiments, the murine MRI measurements, and the ELISA measurements of the Newcastle cohort and cell supernatants and contributed to the preparation of certain depicted items. M.N. performed part of intravital imaging experiments supervised by M.S. A.O.-G., R.C., and C.S.-R performed and recorded the FACS data of the peritonitis model. T.R. was responsible for the acquisition and analysis of the flow cytometry immunophenotyping data as well as of a part of the peritonitis data. R.B. performed measurements of the Utah cohort. V.C. performed the immunostaining of the Rome and Utah cohort while M.M. provided the Rome Cohort and evaluated the immunostaining of the both cohorts. C.G.-G., A.S. and A. Wietelmann were responsible for the operations in the MI model and MRI measurements. C.G.-G. performed the FACS measurements on endothelial membrane and the quantification of adhesion molecule gene expression in murine ECs. J.H. recorded and analyzed flow cytometry data of the HLI model. R.H., J.R.V., and N.D. performed measurements in the Utah cohort. G.G. and K. Stamatelopoulos assisted with advanced statistics. A.M. performed the protein quantification of the Newcastle cohort. W.C. performed the miR-sequencing. S.G. and D.A.S. performed miR-sequencing bioinformatics analysis. S.K. and J.B. provided resources. C.H.S. participated in the recruitment of the Utah cohort. C.T. provided resources and conceptual advice. I.S. provided the Newcastle cohort data. T.B. supervised the work of C.G.-G., A. Wietelmann, and A.S. and provided conceptual advice. A. Gallo supervised the work of V.C., D.A.S., and M.M. and provided conceptual advice. S.G.D. supervised R.B., R.H., J.R.V., and N.D. and provided conceptual advice on the Utah study. S.R.-J. provided resources and conceptual advice. S. Dimmeler provided resources and conceptual advice. M.S. supervised and interpreted the work of M.N. O.S. supervised the work of A.O.-G., R.C., and C.S.-R and designed, performed, analyzed, and interpreted part of the intravital microscopy experiments and provided conceptual advice. All authors discussed the results, commented on and approved the manuscript.

DECLARATION OF INTERESTS

The authors declare no competing interests.

INCLUSION AND DIVERSITY

We support inclusive, diverse, and equitable conduct of research.

Received: March 6, 2022
Revised: January 2, 2023
Accepted: March 30, 2023
Published: April 25, 2023

REFERENCES

1. Wang, Q., Miyakoda, M., Yang, W., Khillan, J., Stachura, D.L., Weiss, M.J., and Nishikura, K. (2004). Stress-induced apoptosis associated with null mutation of ADAR1 RNA editing deaminase gene. J. Biol. Chem. *279*, 4952–4961. https://doi.org/10.1074/jbc.M310162200.
2. Hartner, J.C., Schmittwolf, C., Kispert, A., Müller, A.M., Higuchi, M., and Seeburg, P.H. (2004). Liver disintegration in the mouse embryo caused by deficiency in the RNA-editing enzyme ADAR1. J. Biol. Chem. *279*, 4894–4902. https://doi.org/10.1074/jbc.M311347200.
3. Higuchi, M., Maas, S., Single, F.N., Hartner, J., Rozov, A., Burnashev, N., Feldmeyer, D., Sprengel, R., and Seeburg, P.H. (2000). Point mutation in an AMPA receptor gene rescues lethality in mice deficient in the RNA-editing enzyme ADAR2. Nature *406*, 78–81. https://doi.org/10.1038/35017558.
4. Bass, B.L., and Weintraub, H. (1988). An unwinding activity that covalently modifies its double-stranded RNA substrate. Cell *55*, 1089–1098. https://doi.org/10.1016/0092-8674(88)90253-X.
5. Wagner, R.W., Smith, J.E., Cooperman, B.S., and Nishikura, K. (1989). A double-stranded RNA unwinding activity introduces structural alterations by means of adenosine to inosine conversions in mammalian cells and Xenopus eggs. Proc. Natl. Acad. Sci. USA *86*, 2647–2651. https://doi.org/10.1073/pnas.86.8.2647.
6. Tan, M.H., Li, Q., Shanmugam, R., Piskol, R., Kohler, J., Young, A.N., Liu, K.I., Zhang, R., Ramaswami, G., Ariyoshi, K., et al. (2017). Dynamic landscape and regulation of RNA editing in mammals. Nature *550*, 249–254. https://doi.org/10.1038/nature24041.

Figure 7. Endothelial ADAR2-mediated A-to-I RNA editing of pri-mir-199a-5p and pri-mir-335-3p inhibits Drosha recruitment and consequently miRNA maturation

(A) ADAR2 or IgG (isotype control) RNA immunoprecipitation (IP; RIP) studies followed by quantification of primary miRNAs (pri-miRNA; pri-mirs) expression (n = 4) in HUVECs.

(B) Direct PCR-based miRNA editing studies of pri-mir-199a-1 (top; gray bars), pri-mir-199a-2 (lower left; mid gray bars), and pri-mir-335 (lower right; dark gray bars) in HUVECs transfected with siADAR2 or scrambled revealing the RNA-editing rate per nucleotide with reference to the 5′ end of the mature miRNAs sequence counted as +1 (n = 3–6; depending on site coverage).

(C) Mapping of the most important identified edited sites (black arrows and red font), based on the proximity to Drosha cleavage site (marked with dashed black line), throughout pri-mir-199a-1, pri-mir-199a-2, and pri-mir-335.

(D) The bar chart displays the fold enrichment of the three specific pri-miRNAs in Drosha-precipitates after ADAR2 knockdown compared with scrambled control and after normalization to the respective input and IgG (n = 4).

(E) miR-199a-5p and miR-335-3p expression after co-silencing of ADAR2 and Drosha (n = 4).

(F) Renilla luciferase activity of the relevant *IL6ST* 3′ UTR construct (n = 6).

(G) *IL6ST* mRNA expression (*n* = 4).

(H) Generation of wild-type and edited (A-to-G mutated) pri-mir-199a1 and pri-mir-335 fragment constructs. Stars denote the localization of A-to-G mutations that have been inserted along the hairpins on the sites of the previously identified A-to-I RNA-editing events. See also STAR Methods.

(I and J) *IL6ST* mRNA expression in cells overexpressing the constructs of (H, n = 5).

(K and L) Mature miR-199a-5p (K) and miR-335-3p (L) expression in endothelial cells overexpressing the wild type, edited or the backbone (control^{OE}; pcDNA3.1(+)) pri-mir-199a-1 or pri-mir-335 constructs depicted in (H, n = 5).

Data are presented as mean ± SEM for n biological independent replicates. Experimental groups were compared using a two-tailed Mann-Whitney *U* test or one-way ANOVA followed by Holm-Sidak's multiple comparison test for pairwise comparisons (B). (A–G) *p < 0.05; versus scrambled or IgG IP. $^{\#}$p < 0.05; versus siADAR2. (H–L) *p < 0.05 versus control^{OE} or wild-type pri-mir-199a1/pri-mir-335 as determined by pairwise t test (I and J) or Bonferroni's multiple comparison test (K and L). $^{\#}$p < 0.05 versus wild-type pri-mir-199a1/pri-mir-335 as calculated by Bonferroni's multiple comparison test.

See also Figures S7E–S7H.

7. Bazak, L., Haviv, A., Barak, M., Jacob-Hirsch, J., Deng, P., Zhang, R., Isaacs, F.J., Rechavi, G., Li, J.B., Eisenberg, E., and Levanon, E.Y. (2014). A-to-I RNA editing occurs at over a hundred million genomic sites, located in a majority of human genes. Genome Res. *24*, 365–376. https://doi.org/10.1101/gr.164749.113.

8. Quin, J., Sedmík, J., Vukić, D., Khan, A., Keegan, L.P., and O'Connell, M.A. (2021). ADAR RNA modifications, the epitranscriptome and innate immunity. Trends Biochem. Sci. *46*, 758–771. https://doi.org/10.1016/j.tibs.2021.02.002.

9. Eisenberg, E., and Levanon, E.Y. (2018). A-to-I RNA editing - immune protector and transcriptome diversifier. Nat. Rev. Genet. *19*, 473–490. https://doi.org/10.1038/s41576-018-0006-1.

10. Walkley, C.R., and Li, J.B. (2017). Rewriting the transcriptome: adenosine-to-inosine RNA editing by ADARs. Genome Biol. *18*, 205. https://doi.org/10.1186/s13059-017-1347-3.

11. Nishikura, K. (2016). A-to-I editing of coding and non-coding RNAs by ADARs. Nat. Rev. Mol. Cell Biol. *17*, 83–96. https://doi.org/10.1038/nrm.2015.4.

12. Hwang, T., Park, C.K., Leung, A.K., Gao, Y., Hyde, T.M., Kleinman, J.E., Rajpurohit, A., Tao, R., Shin, J.H., and Weinberger, D.R. (2016). Dynamic regulation of RNA editing in human brain development and disease. Nat. Neurosci. *19*, 1093–1099. https://doi.org/10.1038/nn.4337.

13. Gatsiou, A., and Stellos, K. (2022). RNA modifications in cardiovascular health and disease. Nat. Rev. Cardiol. https://doi.org/10.1038/s41569-022-00804-8.

14. Mannion, N.M., Greenwood, S.M., Young, R., Cox, S., Brindle, J., Read, D., Nellåker, C., Vesely, C., Ponting, C.P., McLaughlin, P.J., et al. (2014). The RNA-editing enzyme ADAR1 controls innate immune responses to RNA. Cell Rep. *9*, 1482–1494. https://doi.org/10.1016/j.celrep.2014.10.041.

15. Liddicoat, B.J., Piskol, R., Chalk, A.M., Ramaswami, G., Higuchi, M., Hartner, J.C., Li, J.B., Seeburg, P.H., and Walkley, C.R. (2015). RNA editing by ADAR1 prevents MDA5 sensing of endogenous dsRNA as nonself. Science *349*, 1115–1120. https://doi.org/10.1126/science.aac7049.

16. Hartner, J.C., Walkley, C.R., Lu, J., and Orkin, S.H. (2009). ADAR1 is essential for the maintenance of hematopoiesis and suppression of interferon signaling. Nat. Immunol. *10*, 109–115. https://doi.org/10.1038/ni.1680.

17. Wang, Q., Khillan, J., Gadue, P., and Nishikura, K. (2000). Requirement of the RNA editing deaminase ADAR1 gene for embryonic erythropoiesis. Science *290*, 1765–1768. https://doi.org/10.1126/science.290.5497.1765.

18. Stellos, K., Gatsiou, A., Stamatelopoulos, K., Perisic Matic, L., John, D., Lunella, F.F., Jaé, N., Rossbach, O., Amrhein, C., Sigala, F., et al. (2016). Adenosine-to-inosine RNA editing controls cathepsin S expression in atherosclerosis by enabling HuR-mediated post-transcriptional regulation. Nat. Med. *22*, 1140–1150. https://doi.org/10.1038/nm.4172.

19. Forbes, S.J., and Rosenthal, N. (2014). Preparing the ground for tissue regeneration: from mechanism to therapy. Nat. Med. *20*, 857–869. https://doi.org/10.1038/nm.3653.

20. Springer, T.A. (1994). Traffic signals for lymphocyte recirculation and leukocyte emigration: the multistep paradigm. Cell *76*, 301–314.

21. Friedl, P., and Weigelin, B. (2008). Interstitial leukocyte migration and immune function. Nat. Immunol. *9*, 960–969. https://doi.org/10.1038/ni.f.212.

22. Ley, K., and Kansas, G.S. (2004). Selectins in T-cell recruitment to non-lymphoid tissues and sites of inflammation. Nat. Rev. Immunol. *4*, 325–335. https://doi.org/10.1038/nri1351.

23. Romano, M., Sironi, M., Toniatti, C., Polentarutti, N., Fruscella, P., Ghezzi, P., Faggioni, R., Luini, W., van Hinsbergh, V., Sozzani, S., et al. (1997). Role of IL-6 and its soluble receptor in induction of chemokines and leukocyte recruitment. Immunity *6*, 315–325.

24. Schuett, H., Oestreich, R., Waetzig, G.H., Annema, W., Luchtefeld, M., Hillmer, A., Bavendiek, U., von Felden, J., Divchev, D., Kempf, T., et al. (2012). Transsignaling of interleukin-6 crucially contributes to atherosclerosis in mice. Arterioscler. Thromb. Vasc. Biol. *32*, 281–290. https://doi.org/10.1161/ATVBAHA.111.229435.

25. Rakemann, T., Niehof, M., Kubicka, S., Fischer, M., Manns, M.P., Rose-John, S., and Trautwein, C. (1999). The designer cytokine hyper-interleukin-6 is a potent activator of STAT3-dependent gene transcription in vivo and in vitro. J. Biol. Chem. *274*, 1257–1266. https://doi.org/10.1074/jbc.274.3.1257.

26. Modur, V., Li, Y., Zimmerman, G.A., Prescott, S.M., and McIntyre, T.M. (1997). Retrograde inflammatory signaling from neutrophils to endothelial cells by soluble interleukin-6 receptor alpha. J. Clin. Invest. *100*, 2752–2756. https://doi.org/10.1172/JCI119821.

27. Fischer, M., Goldschmitt, J., Peschel, C., Brakenhoff, J.P., Kallen, K.J., Wollmer, A., Grötzinger, J., and Rose-John, S. (1997). I. A bioactive designer cytokine for human hematopoietic progenitor cell expansion. Nat. Biotechnol. *15*, 142–145. https://doi.org/10.1038/nbt0297-142.

28. Sironi, M., Breviario, F., Proserpio, P., Biondi, A., Vecchi, A., Van Damme, J., Dejana, E., and Mantovani, A. (1989). IL-1 stimulates IL-6 production in endothelial cells. J. Immunol. *142*, 549–553.

29. Klouche, M., Bhakdi, S., Hemmes, M., and Rose-John, S. (1999). Novel path to activation of vascular smooth muscle cells: up-regulation of gp130 creates an autocrine activation loop by IL-6 and its soluble receptor. J. Immunol. *163*, 4583–4589.

30. Rose-John, S. (2018). Interleukin-6 family cytokines. Cold Spring Harb. Perspect. Biol. *10*. https://doi.org/10.1101/cshperspect.a028415.

31. Taniguchi, K., Wu, L.W., Grivennikov, S.I., de Jong, P.R., Lian, I., Yu, F.X., Wang, K., Ho, S.B., Boland, B.S., Chang, J.T., et al. (2015). A gp130-Src-YAP module links inflammation to epithelial regeneration. Nature *519*, 57–62. https://doi.org/10.1038/nature14228.

32. Epelman, S., Liu, P.P., and Mann, D.L. (2015). Role of innate and adaptive immune mechanisms in cardiac injury and repair. Nat. Rev. Immunol. *15*, 117–129. https://doi.org/10.1038/nri3800.

33. van der Kwast, R.V.C.T., Parma, L., van der Bent, M.L., van Ingen, E., Baganha, F., Peters, H.A.B., Goossens, E.A.C., Simons, K.H., Palmen, M., de Vries, M.R., et al. (2020). Adenosine-to-inosine editing of vasoactive microRNAs alters their targetome and function in ischemia. Mol. Ther. Nucleic Acids *21*, 932–953. https://doi.org/10.1016/j.omtn.2020.07.020.

34. Jostock, T., Müllberg, J., Ozbek, S., Atreya, R., Blinn, G., Voltz, N., Fischer, M., Neurath, M.F., and Rose-John, S. (2001). Soluble gp130 is the natural inhibitor of soluble interleukin-6 receptor transsignaling responses. Eur. J. Biochem. *268*, 160–167. https://doi.org/10.1046/j.1432-1327.2001.01867.x.

35. Vivier, E., Tomasello, E., Baratin, M., Walzer, T., and Ugolini, S. (2008). Functions of natural killer cells. Nat. Immunol. *9*, 503–510. https://doi.org/10.1038/ni1582.

36. Kawahara, Y., Zinshteyn, B., Sethupathy, P., Iizasa, H., Hatzigeorgiou, A.G., and Nishikura, K. (2007). Redirection of silencing targets by adenosine-to-inosine editing of miRNAs. Science *315*, 1137–1140. https://doi.org/10.1126/science.1138050.

37. Cesarini, V., Silvestris, D.A., Tassinari, V., Tomaselli, S., Alon, S., Eisenberg, E., Locatelli, F., and Gallo, A. (2018). ADAR2/miR-589-3p axis controls glioblastoma cell migration/invasion. Nucleic Acids Res. *46*, 2045–2059. https://doi.org/10.1093/nar/gkx1257.

38. Yang, W., Chendrimada, T.P., Wang, Q., Higuchi, M., Seeburg, P.H., Shiekhattar, R., and Nishikura, K. (2006). Modulation of microRNA processing and expression through RNA editing by ADAR deaminases. Nat. Struct. Mol. Biol. *13*, 13–21. https://doi.org/10.1038/nsmb1041.

39. Ota, H., Sakurai, M., Gupta, R., Valente, L., Wulff, B.E., Ariyoshi, K., Iizasa, H., Davuluri, R.V., and Nishikura, K. (2013). ADAR1 forms a complex with Dicer to promote microRNA processing and RNA-induced gene silencing. Cell *153*, 575–589. https://doi.org/10.1016/j.cell.2013.03.024.

40. Tomaselli, S., Galeano, F., Alon, S., Raho, S., Galardi, S., Polito, V.A., Presutti, C., Vincenti, S., Eisenberg, E., Locatelli, F., and Gallo, A. (2015). Modulation of microRNA editing, expression and processing by ADAR2

deaminase in glioblastoma. Genome Biol. *16*, 5. https://doi.org/10.1186/s13059-014-0575-z.

41. Lee, Y., Ahn, C., Han, J., Choi, H., Kim, J., Yim, J., Lee, J., Provost, P., Rådmark, O., Kim, S., and Kim, V.N. (2003). The nuclear RNase III Drosha initiates microRNA processing. Nature *425*, 415–419. https://doi.org/10.1038/nature01957.
42. Vlachogiannis, N.I., Sachse, M., Georgiopoulos, G., Zormpas, E., Bampatsias, D., Delialis, D., Bonini, F., Galyfos, G., Sigala, F., Stamatelopoulos, K., et al. (2021). Adenosine-to-inosine Alu RNA editing controls the stability of the pro-inflammatory long noncoding RNA NEAT1 in atherosclerotic cardiovascular disease. J. Mol. Cell. Cardiol. *160*, 111–120. https://doi.org/10.1016/j.yjmcc.2021.07.005.
43. Vlachogiannis, N.I., Gatsiou, A., Silvestris, D.A., Stamatelopoulos, K., Tektonidou, M.G., Gallo, A., Sfikakis, P.P., and Stellos, K. (2020). Increased adenosine-to-inosine RNA editing in rheumatoid arthritis. J. Autoimmun. *106*, 102329. https://doi.org/10.1016/j.jaut.2019.102329.
44. Vlachogiannis, N.I., Tual-Chalot, S., Zormpas, E., Bonini, F., Ntouros, P.A., Pappa, M., Bournia, V.K., Tektonidou, M.G., Souliotis, V.L., Mavragani, C.P., et al. (2021). Adenosine-to-inosine RNA editing contributes to type I interferon responses in systemic sclerosis. J. Autoimmun. *125*, 102755. https://doi.org/10.1016/j.jaut.2021.102755.
45. Gomez-Salinero, J.M., and Rafii, S. (2018). Endothelial cell adaptation in regeneration. Science *362*, 1116–1117. https://doi.org/10.1126/science.aar4800.
46. Nowell, M.A., Richards, P.J., Fielding, C.A., Ognjanovic, S., Topley, N., Williams, A.S., Bryant-Greenwood, G., and Jones, S.A. (2006). Regulation of pre-B cell colony-enhancing factor by STAT-3-dependent interleukin-6 trans-signaling: implications in the pathogenesis of rheumatoid arthritis. Arthritis Rheum. *54*, 2084–2095. https://doi.org/10.1002/art.21942.
47. Zhang, H., Neuhöfer, P., Song, L., Rabe, B., Lesina, M., Kurkowski, M.U., Treiber, M., Wartmann, T., Regnér, S., Thorlacius, H., et al. (2013). IL-6 trans-signaling promotes pancreatitis-associated lung injury and lethality. J. Clin. Invest. *123*, 1019–1031. https://doi.org/10.1172/JCI64931.
48. Mitsuyama, K., Matsumoto, S., Rose-John, S., Suzuki, A., Hara, T., Tomiyasu, N., Handa, K., Tsuruta, O., Funabashi, H., Scheller, J., et al. (2006). STAT3 activation via interleukin 6 trans-signalling contributes to ileitis in SAMP1/Yit mice. Gut *55*, 1263–1269. https://doi.org/10.1136/gut.2005.079343.
49. Jones, S.A., Scheller, J., and Rose-John, S. (2011). Therapeutic strategies for the clinical blockade of IL-6/gp130 signaling. J. Clin. Invest. *121*, 3375–3383. https://doi.org/10.1172/JCI57158.
50. Garbers, C., Heink, S., Korn, T., and Rose-John, S. (2018). Interleukin-6: designing specific therapeutics for a complex cytokine. Nat. Rev. Drug Discov. *17*, 395–412. https://doi.org/10.1038/nrd.2018.45.
51. Cormack, S., Mohammed, A., Panahi, P., Das, R., Steel, A.J., Chadwick, T., Bryant, A., Egred, M., Stellos, K., and Spyridopoulos, I.; CAPRI investigators (2020). Effect of ciclosporin on safety, lymphocyte kinetics and left ventricular remodelling in acute myocardial infarction. Br. J. Clin. Pharmacol. *86*, 1387–1397. https://doi.org/10.1111/bcp.14252.
52. Pasotti, M., Prati, F., and Arbustini, E. (2006). The pathology of myocardial infarction in the pre- and post-interventional era. Heart *92*, 1552–1556. https://doi.org/10.1136/hrt.2005.086934.
53. Uretsky, B.F., Thygesen, K., Armstrong, P.W., Cleland, J.G., Horowitz, J.D., Massie, B.M., Packer, M., Poole-Wilson, P.A., and Ryden, L. (2000). Acute coronary findings at autopsy in heart failure patients with sudden death: results from the assessment of treatment with lisinopril and survival (ATLAS) trial. Circulation *102*, 611–616.
54. Wever-Pinzon, J., Selzman, C.H., Stoddard, G., Wever-Pinzon, O., Catino, A., Kfoury, A.G., Diakos, N.A., Reid, B.B., McKellar, S., Bonios, M., et al. (2016). Impact of ischemic heart failure etiology on cardiac recovery during mechanical unloading. J. Am. Coll. Cardiol. *68*, 1741–1752. https://doi.org/10.1016/j.jacc.2016.07.756.
55. Drakos, S.G., Wever-Pinzon, O., Selzman, C.H., Gilbert, E.M., Alharethi, R., Reid, B.B., Saidi, A., Diakos, N.A., Stoker, S., Davis, E.S., et al. (2013). Magnitude and time course of changes induced by continuous-flow left ventricular assist device unloading in chronic heart failure: insights into cardiac recovery. J. Am. Coll. Cardiol. *61*, 1985–1994. https://doi.org/10.1016/j.jacc.2013.01.072.
56. Pitulescu, M.E., Schmidt, I., Benedito, R., and Adams, R.H. (2010). Inducible gene targeting in the neonatal vasculature and analysis of retinal angiogenesis in mice. Nat. Protoc. *5*, 1518–1534. https://doi.org/10.1038/nprot.2010.113.
57. Hideyama, T., Yamashita, T., Suzuki, T., Tsuji, S., Higuchi, M., Seeburg, P.H., Takahashi, R., Misawa, H., and Kwak, S. (2010). Induced loss of ADAR2 engenders slow death of motor neurons from Q/R site-unedited GluR2. J. Neurosci. *30*, 11917–11925. https://doi.org/10.1523/JNEUROSCI.2021-10.2010.
58. Betz, U.A., Bloch, W., van den Broek, M., Yoshida, K., Taga, T., Kishimoto, T., Addicks, K., Rajewsky, K., and Müller, W. (1998). Postnatally induced inactivation of gp130 in mice results in neurological, cardiac, hematopoietic, immunological, hepatic, and pulmonary defects. J. Exp. Med. *188*, 1955–1965. https://doi.org/10.1084/jem.188.10.1955.
59. Santander, N., Lizama, C.O., Meky, E., McKinsey, G.L., Jung, B., Sheppard, D., Betsholtz, C., and Arnold, T.D. (2020). Lack of Flvcr2 impairs brain angiogenesis without affecting the blood-brain barrier. J. Clin. Invest. *130*, 4055–4068. https://doi.org/10.1172/JCI136578.
60. Chen, Q., Liu, Y., Jeong, H.W., Stehling, M., Dinh, V.V., Zhou, B., and Adams, R.H. (2019). Apelin(+) endothelial niche cells control hematopoiesis and mediate vascular regeneration after myeloablative injury. Cell Stem Cell *25*. 768.e6–783.e6. https://doi.org/10.1016/j.stem.2019.10.006.
61. Liu, M., Zhang, L., Marsboom, G., Jambusaria, A., Xiong, S., Toth, P.T., Benevolenskaya, E.V., Rehman, J., and Malik, A.B. (2019). Sox17 is required for endothelial regeneration following inflammation-induced vascular injury. Nat. Commun. *10*, 2126. https://doi.org/10.1038/s41467-019-10134-y.
62. Manavski, Y., Abel, T., Hu, J., Kleinlützum, D., Buchholz, C.J., Belz, C., Augustin, H.G., Boon, R.A., and Dimmeler, S. (2017). Endothelial transcription factor KLF2 negatively regulates liver regeneration via induction of activin A. Proc. Natl. Acad. Sci. USA *114*, 3993–3998. https://doi.org/10.1073/pnas.1613392114.
63. Hergenreider, E., Heydt, S., Tréguer, K., Boettger, T., Horrevoets, A.J., Zeiher, A.M., Scheffer, M.P., Frangakis, A.S., Yin, X., Mayr, M., et al. (2012). Atheroprotective communication between endothelial cells and smooth muscle cells through miRNAs. Nat. Cell Biol. *14*, 249–256. https://doi.org/10.1038/ncb2441.
64. Marin, V., Montero-Julian, F.A., Grès, S., Boulay, V., Bongrand, P., Farnarier, C., and Kaplanski, G. (2001). The IL-6-soluble IL-6Ralpha autocrine loop of endothelial activation as an intermediate between acute and chronic inflammation: an experimental model involving thrombin. J. Immunol. *167*, 3435–3442.
65. Stellos, K., Langer, H., Gnerlich, S., Panagiota, V., Paul, A., Schönberger, T., Ninci, E., Menzel, D., Mueller, I., Bigalke, B., et al. (2010). Junctional adhesion molecule A expressed on human CD34+ cells promotes adhesion on vascular wall and differentiation into endothelial progenitor cells. Arterioscler. Thromb. Vasc. Biol. *30*, 1127–1136. https://doi.org/10.1161/ATVBAHA.110.204370.
66. Li, N., You, X., Chen, T., Mackowiak, S.D., Friedländer, M.R., Weigt, M., Du, H., Gogol-Döring, A., Chang, Z., Dieterich, C., et al. (2013). Global profiling of miRNAs and the hairpin precursors: insights into miRNA processing and novel miRNA discovery. Nucleic Acids Res. *41*, 3619–3634. https://doi.org/10.1093/nar/gkt072.
67. Kuenne, C., Preussner, J., Herzog, M., Braun, T., and Looso, M. (2014). MIRPIPE: quantification of microRNAs in niche model organisms. Bioinformatics *30*, 3412–3413. https://doi.org/10.1093/bioinformatics/btu573.
68. Alon, S., Erew, M., and Eisenberg, E. (2015). DREAM: a webserver for the identification of editing sites in mature miRNAs using deep sequencing data. Bioinformatics *31*, 2568–2570. https://doi.org/10.1093/bioinformatics/btv187.

69. Picardi, E., and Pesole, G. (2013). REDItools: high-throughput RNA editing detection made easy. Bioinformatics *29*, 1813–1814. https://doi.org/10.1093/bioinformatics/btt287.

70. Martin, M. (2011). Cutadapt removes adapter sequences from high-throughput sequencing reads. EMBnet.journal *17*, 3. https://doi.org/10.14806/ej.17.1.200.

71. Andrews, S. (2010). FastQC: a quality control tool for high throughput sequence data. https://www.bioinformatics.babraham.ac.uk/projects/fastqc/.

72. Ewels, P., Magnusson, M., Lundin, S., and Käller, M. (2016). MultiQC: summarize analysis results for multiple tools and samples in a single report. Bioinformatics *32*, 3047–3048. https://doi.org/10.1093/bioinformatics/btw354.

73. Yates, A.D., Achuthan, P., Akanni, W., Allen, J., Allen, J., Alvarez-Jarreta, J., Amode, M.R., Armean, I.M., Azov, A.G., Bennett, R., et al. (2020). Ensembl 2020. Nucleic Acids Res. *48*, D682–D688. https://doi.org/10.1093/nar/gkz966.

74. Dobin, A., Davis, C.A., Schlesinger, F., Drenkow, J., Zaleski, C., Jha, S., Batut, P., Chaisson, M., and Gingeras, T.R. (2013). STAR: ultrafast universal RNA-seq aligner. Bioinformatics *29*, 15–21. https://doi.org/10.1093/bioinformatics/bts635.

75. Anders, S., Pyl, P.T., and Huber, W. (2015). HTSeq–a Python framework to work with high-throughput sequencing data. Bioinformatics Oxf. Engl. *31*, 166–169. https://doi.org/10.1093/bioinformatics/btu638.

76. Love, M.I., Huber, W., and Anders, S. (2014). Moderated estimation of fold change and dispersion for RNA-seq data with DESeq2. Genome Biol. *15*, 550.

77. Krämer, A., Green, J., Pollard, J., Jr., and Tugendreich, S. (2014). Causal analysis approaches in ingenuity pathway analysis. Bioinformatics *30*, 523–530. https://doi.org/10.1093/bioinformatics/btt703.

78. Kozomara, A., Birgaoanu, M., and Griffiths-Jones, S. (2019). miRBase: from microRNA sequences to function. Nucleic Acids Res. *47*, D155–D162. https://doi.org/10.1093/nar/gky1141.

79. Kawahara, Y. (2012). Quantification of adenosine-to-inosine editing of microRNAs using a conventional method. Nat. Protoc. *7*, 1426–1437. https://doi.org/10.1038/nprot.2012.073.

80. Lukas, D., Yogev, N., Kel, J.M., Regen, T., Mufazalov, I.A., Tang, Y., Wanke, F., Reizis, B., Müller, W., Kurschus, F.C., et al. (2017). TGF-beta inhibitor Smad7 regulates dendritic cell-induced autoimmunity. Proc. Natl. Acad. Sci. USA *114*, E1480–E1489. https://doi.org/10.1073/pnas.1615065114.

81. Heink, S., Yogev, N., Garbers, C., Herwerth, M., Aly, L., Gasperi, C., Husterer, V., Croxford, A.L., Möller-Hackbarth, K., Bartsch, H.S., et al. (2017). Trans-presentation of IL-6 by dendritic cells is required for the priming of pathogenic TH17 cells. Nat. Immunol. *18*, 74–85. https://doi.org/10.1038/ni.3632.

82. Ortega-Gomez, A., Salvermoser, M., Rossaint, J., Pick, R., Brauner, J., Lemnitzer, P., Tilgner, J., de Jong, R.J., Megens, R.T., Jamasbi, J., et al. (2016). Cathepsin G controls arterial but not venular myeloid cell recruitment. Circulation *134*, 1176–1188. https://doi.org/10.1161/CIRCULATIONAHA.116.024790.

83. Lörchner, H., Pöling, J., Gajawada, P., Hou, Y., Polyakova, V., Kostin, S., Adrian-Segarra, J.M., Boettger, T., Wietelmann, A., Warnecke, H., et al. (2015). Myocardial healing requires Reg3beta-dependent accumulation of macrophages in the ischemic heart. Nat. Med. *21*, 353–362. https://doi.org/10.1038/nm.3816.

84. Bonauer, A., Carmona, G., Iwasaki, M., Mione, M., Koyanagi, M., Fischer, A., Burchfield, J., Fox, H., Doebele, C., Ohtani, K., et al. (2009). MicroRNA-92a controls angiogenesis and functional recovery of ischemic tissues in mice. Science *324*, 1710–1713. https://doi.org/10.1126/science.1174381.

85. Klotzsche-von Ameln, A., Cremer, S., Hoffmann, J., Schuster, P., Khedr, S., Korovina, I., Troullinaki, M., Neuwirth, A., Sprott, D., Chatzigeorgiou, A., et al. (2017). Endogenous developmental endothelial locus-1 limits ischaemia-related angiogenesis by blocking inflammation. Thromb. Haemost. *117*, 1150–1163. https://doi.org/10.1160/TH16-05-0354.

STAR★METHODS

KEY RESOURCES TABLE

REAGENT or RESOURCE	SOURCE	IDENTIFIER
Antibodies		
Anti-laminin antibody (1:200)	Abcam	Cat# ab11575; RRID:AB_298179
Goat Anti-Armenian hamster (1:200)	Abcam	Cat# ab173003; RRID:AB_2936402
CD44 (FACS; 1:200)	BD Biosciences	Cat# 553131; RRID:AB_394646
CD25 (FACS; 1:200)	BD Biosciences	Cat# 553068; RRID:AB_394600
CD8a (FACS; 1:500)	BD Biosciences	Cat# 553028; RRID:AB_394566
CD62L (FACS; 1:200)	BD Biosciences	Cat# 612833; RRID:AB_2870155
CD90.2 (FACS; 1:1000)	BD Biosciences	Cat# 553000; RRID:AB_394539
CD4 (FACS; 1:300)	BD Biosciences	Cat# 940108; RRID:AB_2875998
CD45 (staining; 1:100)	BD Biosciences	Cat# 553076; RRID:AB_394606
CD62E (staining; 1:100)	BD Biosciences	Cat# 550290; RRID:AB_393585
ICAM-1 (staining; 1:100)	BD Biosciences	Cat# 553250; RRID:AB_394732
CD31 (staining; 1:100)	BD Biosciences	Cat# 550274; RRID:AB_393571
CD11b (FACS; 1:1000)	BD Biosciences	Cat# 612800; RRID:AB_2870127
Ly6C (FACS; 1:100)	BD Biosciences	Cat# 557359; RRID:AB_396663
IgM (FACS; 1:200)	BD Biosciences	Cat# 550588; RRID:AB_393767
CD138 (FACS; 1:50)	BD Biosciences	Cat# 940137; RRID:AB_2876026
Purified Rat anti-mouse CD144 (cell isolation; 3 μg/ml)	BD Pharmigen	Cat# 555289; RRID:AB_395707
Rabbit polyclonal Drosha Antibody (WB, IP; 5 μg)	Bethyl Laboratories	Cat# A301-886A; RRID:AB_1309798
Ly6G (*in vivo* peritonitis; 1:200)	Biolegend	Cat# 108428; RRID:AB_893558
Ly6C (*in vivo* peritonitis; 1:200)	Biolegend	Cat# 128006; RRID:AB_1186135
CD45 (*In Vivo* Peritonitis; 1:200)	Biolegend	Cat# 103116; RRID:AB_312981
Ly6G (IVM; 1 μg/mouse)	Biolegend	Cat# 127608; RRID:AB_1186099
Ly6C (IVM; 1 μg/mouse)	Biolegend	Cat# 128022; RRID:AB_10639728
Ly6G (FACS; 1:1000)	Biolegend	Cat# 127602; RRID:AB_1089180
B220 (FACS; 1:400)	Biolegend	Cat# 103201; RRID:AB_312986
NK 1.1 (FACS; 1:100)	Biolegend	Cat# 108701; RRID:AB_313388
CD19 (FACS; 1:200)	Biolegend	Cat# 101505; RRID:AB_312824
TCR γδ (FACS; 1:200)	Biolegend	Cat# 118105; RRID:AB_313829
TCR β (FACS; 1:400)	Biolegend	Cat# 109207; RRID:AB_313430
Streptavidin (FACS; 1:200)	Biolegend	Cat# 405213; RRID: AB_2936403
STAT3 (D3Z2G) rabbit mAb (1:1000)	Cell Signalling	Cat# 12640; RRID:AB_2629499
p-STAT3 (D3A7) rabbit mAb (1:2000)	Cell Signalling	Cat# 9145; RRID:AB_2491009
α-Tubulin Antibody (1:1000)	Cell Signalling	Cat# 2144; RRID:AB_2210548
Anti-CD31 (human cohort IHC; 1:100)	Dako	Cat# GA610; RRID:AB_2892053
Anti-CD43 (human cohort IHC; 1:100)	Dako	Cat# GA63661-2; RRID:AB_2936404
Anti-CD45-LCA (human cohort IHC; 1:200)	Dako	Cat# M070101-2; RRID:AB_2750582
Foxp3^{-} (FACS; 1:200)	eBioscience	Cat# 12-5773-82; RRID:AB_465936
F4/80 (FACS) 1:100	eBioscience	Cat# 12-4801-82; RRID:AB_465923
CD11b (IVM; 1 μg/mouse)	eBioscience	Cat# 12-0112-85; RRID:AB_465549
F4/80 (*in vivo* peritonitis; 1:200)	eBioscience	Cat# 17-4801-82; RRID:AB_2784648
CD11b (*in vivo* peritonitis; 1:200)	eBioscience	Cat# 48-0112-82; RRID:AB_1582236
CD115 (*in vivo* peritonitis; 1:200)	eBioscience	Cat# 12-1152-82; RRID:AB_465808
Streptavidin (FACS; 1:200)	eBioscience;	Cat# 47-4317-82; RRID:AB_10366688
MCP-1 (staining; 1:100)	eBiosciences	Cat# 11-7096-81; RRID:AB_465399

(*Continued on next page*)

Continued

REAGENT or RESOURCE	SOURCE	IDENTIFIER
Goat anti-rat Alexa 568 (1:200)	Invitrogen	Cat# A-11077; RRID:AB_2534121
Goat anti-rat Alexa 488 (1:200)	Invitrogen	Cat# A-11006; RRID:AB_2534074
Streptavidin, AlexaFluor488 conjugate (1:200)	Invitrogen	Cat# S11223; RRID:AB_2936405
IgG (H+L) AlexaFluor 647 (1:200)	Invitrogen	Cat# A-21245; RRID:AB_2535813
Anti-gp130 rabbit polyclonal (IgG 2 μg/ml)	Millipore	Cat# 06-291; RRID:AB_310091
VCAM-1 (staining; 1:50)	R&D Systems	Cat# MAB6432; RRID:AB_2214051
Anti-ADAR2 (human cohort IHC; 1:50)	Santa Cruz Biotechnology	Cat# sc-73409; RRID:AB_2289194
Anti-IL6ST (human cohort IHC; 1:100)	Santa Cruz Biotechnology	Cat# sc-376280; RRID:AB_10986409
Monoclonal anti-actin α smooth muscle-Cy3 clone 1A4 (1:400)	SigmaAldrich	Cat# C6198; RRID:AB_476856
Mouse ADAR2 antibody (WB; 5 μg/ml)	SigmaAldrich	Cat# SAB1405426; RRID:AB_10740297
Anti-ADAR2 (WB, IP; 1:100, 5 μg)	SigmaAldrich/Atlas antibodies	Cat# HPA018277; RRID:AB_1844591
Biotinylated Isolectin B4 (1:50)	Vector Laboratories and Molecular Probes	Cat# B-1205; RRID:AB_2314661
Biological samples		
Heart tissues from subjects with acute myocardial infarction	Histological archive of the Fondazione Policlinico Universitario "A. Gemelli", IRCCS, UOC Anatomia Patologica, Italy, Rome	IRB number: 30075/19; 2695
Serum samples from subjects with human acute myocardial infarction	Newcastle Clinical Trials Unit	Cormack et al.[51]; IRB number: 14/NE/1070; Clinical trial registry: NCT02390674
Heart tissue from Patients diagnosed with chronic ischemic heart disease and end-stage heart failure who underwent implantation of a continuous-flow left ventricular assist device	University of Utah Hospitals and Clinics, USA	Pasotti et al.[52]; IRB number: 00030622; Clinical trial registry: NCT01099982
Chemicals, peptides, and recombinant proteins		
Fc blocking solution	eBiosciences	Cat# 14-9161-73
Fixable Viability Dye eFluor™ 450	eBioscience	Cat# 65-0863-14
Dulbecco's phosphate-buffered saline (DPBS)	Gibco	Cat# 14190144
phosphate buffered saline (PBS)	Gibco	Cat# 10010023
Trypan Blue	Gibco	Cat# I5250-061
EGM Endothelial Cell Growth Medium	Lonza	Cat# CC-3124
Lipofectamine 2000	Invitrogen	Cat# 11668019
Lipofectamine RNAiMax	Invitrogen	Cat# 13778150
Recombinant Human IL-6/IL-6R alpha Protein Chimera	R&D Systems	Cat# 8954-SR-025
Recombinant Human IL-11 Protein	R&D Systems	Cat# 218-IL-005
Recombinant Human IL-27 Protein	R&D Systems	Cat# 2526-IL-010
Recombinant Human Cardiotrophin-1/CT-1 Protein	R&D Systems	Cat# 612-CD-010
Recombinant Human LIF Protein	R&D Systems	Cat# 7734-LF-025
Recombinant Human Oncostatin M (OSM) Protein	R&D Systems	Cat# 295-OM-010
Recombinant Mouse IL-6/IL-6R alpha Protein Chimera	R&D Systems	Cat# 9038-SR-025
Recombinant Human IL-6 Protein	R&D Systems	Cat# 206-IL-050
Recombinant Human IL-6R alpha Protein	R&D Systems	Cat# 227-SR-025
Formaldehyde	Roth	Cat# 4979.1
Actinomycin D	Sigma-Aldrich	Cat# A1410
Tamoxifen	Sigma-Aldrich	Cat# T5648
Bovine Serum Albumin	Sigma-Aldrich	Cat# A9418
4-OH Tamoxifen	Sigma-Aldrich	Cat# H6278

(*Continued on next page*)

Continued

REAGENT or RESOURCE	SOURCE	IDENTIFIER
Hanks Balanced Salt Solution (HBSS)	Thermo Scientific	Cat# 88284
DAPI	Thermofisher	Cat# P36935
Critical commercial assays		
Masson's trichrome staining	Abcam	Cat# ab150686
Bio-Plex Pro Human Cytokine IL-6 Set	BioRad	Cat#171B5006M
EnVision FLEX Target Retrieval Solution kits	Dako	Cat# K800521-2
1X RBC Lysis Buffer	eBiosciences	Cat# 00-4333-57
Luminex-based Multiplex Immunoassays (Human Cytokine /Chemokine Panel	Eve Technologies, Alberta, Canada	Cat# HD71
Mouse Cytokine/Chemokine Panel	Eve Technologies, Alberta, Canada	Cat# MD44
CountBright™ absolute counting beads	Invitrogen	Cat# C36950
MILLIPLEX MAP Human High Sensitivity T Cell Panel Premixed 13-plex - Immunology Multiplex Assay	Millipore	Cat# HSTCMAG28SPMX13
Skeletal Muscle Dissociation Kit	Miltenyi Biotec	Cat# 130-098-305
miRNeasy Mini kit	Qiagen	Cat# 217004
Human IL-6R alpha Quantikine ELISA Kit	R&D Systems	Cat# DR600
Magna RIP™ RNA-Binding Protein Immunoprecipitation Kit	Sigma-Aldrich	Cat# 17-700
RedExtractNAmp kit	Sigma Aldrich	Cat# R4775
M-MLV reverse transcriptase	ThermoScientific	Cat# 28025013
Restore Western blot Stripping Buffer	ThermoScientific	Cat# 21059
Direct-zol RNA MiniPrep kit	Zymoresearch	Cat# R2053
Deposited data		
Total RNA sequencing data	Stellos et al.[18]	GEO: GSE60217
Small RNA-sequencing data	This paper	GEO: GSE105091
Experimental models: Cell lines		
Primary human umbilical vein endothelial cells (HUVECs)	Lonza	Cat# CC-2935
Primary murine endothelial cells	This paper	N/A
Non-primary murine endothelial cells, H5V	Uretsky et al.[53]	RRID: CVCL_AZ87
Experimental models: Organisms/strains		
B6.129-Adarb1"tm1Phs/Gria2"tm1.1Phs""	Higuchi et al.[3]	RRID:MMRRC_034679-UNC
Adarb1"tm1.1Skwa"	Wever-Pinzon et al.[54]	MGI:4840554
Tg(Cdh5-Cre/ERT2)1Rha/J	Drakos et al.[55]	MGI:3848982
Il6st "tm1Wme"/B6.129(Cg)-Gt(ROSA)26Sortm4(ACTB-tdTomato,-EGFP)Luo/J	Prof. Christian Trautwein (Aachen University, Germany) and Pitulescu et al.[56]	N/A
Il6st "tm1Wme"- Tg(Cdh5-cre/ERT2)1Rha -Gt(ROSA)26Sor "tm4(ACTB-tdTomato,-EGFP)Luo"/J	This paper	N/A
C57BL/6NCtrl	Charles River	RRID:IMSR_CRL:027
B6.129-Adar"tm1Knk"/Mmjax	The Jackson Laboratory	RRID:MMRRC_034619-JAX
Oligonucleotides		
siRNA, precursor and LNA-miRNA assays, see Table S5	This paper	N/A
Primer/Assay Name, see Table S5	This paper	N/A
Recombinant DNA		
pcDNA 3.1 (+) plasmid	Invitrogen	Cat#V79020
psiCheck2 vector	Promega	Cat#C802A
pCMV6-Entry vector	Origene	Cat#RC209073
pri-mir plasmids	This paper	N/A

(*Continued on next page*)

Continued

REAGENT or RESOURCE	SOURCE	IDENTIFIER
IL6ST plasmid	This paper	N/A
IL6ST 3'UTR plasmid	This paper	N/A
ADAR2 plasmid	This paper	N/A
Software and algorithms		
Cutadapt	Martin[57]	https://cutadapt.readthedocs.io/en/stable/
FACSDiva software (BD)	BDBiosciences	N/A
DAVID	N/A	https://david-d.ncifcrf.gov/
DESeq2	Betz et al.[58]	https://bioconductor.org/packages/release/bioc/html/DESeq2.html
Ensembl	Santander et al.[59]	https://www.ensembl.org/index.html
FASTQC	Chen et al.[60]	https://www.bioinformatics.babraham.ac.uk/projects/fastqc/
FlowJo	N/A	https://www.flowjo.com/
FIJI software	N/A	https://imagej.net/software/fiji/downloads
GraphPad Prism	N/A	https://www.graphpad.com/
Image J software	N/A	https://imagej.nih.gov/ij/
Ingenuity Pathway Analysis® tool	QIAGEN	N/A
MiRWalk	N/A	http://zmf.umm.uni-heidelberg.de/apps/zmf/mirwalk2
miRBase	Liu et et al.[61]	http://mirbase.org/
MultiQC	Manavski et al.[62]	https://multiqc.info/
R	N/A	https://www.r-project.org/
STAR aligner	Hergenreider et al.[63]	https://github.com/alexdobin/STAR

RESOURCE AVAILABILITY

Lead contact

Additional information and requests for resources and reagents should be directed to and will be fulfilled by the lead contact Konstantinos Stellos (konstantinos.stellos@medma.uni-heidelberg.de).

Materials availability

Reagents, plasmids and mouse lines reported in this study are available upon signing a Materials Transfer Agreement.

Data and code availability

- The RNA-seq data have been deposited at GEO and are publicly available as of the date of publication. Accession numbers are listed in the key resources table.
- No original code has been reported in this paper.
- Any additional information required to reanalyze the data reported in this paper is available from the lead contact upon request. Restrictions can apply in regards to confidential medical records.

EXPERIMENTAL MODEL AND STUDY PARTICIPANT DETAILS

Acute myocardial infarction cohort/ Newcastle Cohort

Serum samples were derived from a well-characterized human acute myocardial infarction (AMI) cohort [sub-cohort of n=47 patients from the CAPRI trial (NCT02390674) with available cardiac magnetic resonance (CMR) imaging conducted in the UK].[51] In the CAPRI trial patients with acute ST-segment elevation myocardial infarction (STEMI) with symptom onset of < 6 h and blocked culprit artery were randomised to receive either ciclosporin or placebo before reperfusion (primary percutaneous coronary intervention). CAPRI trial was conducted in accordance with the principles of Good Clinical Practice and was ethically approved by the National Research Ethics Committee North-East—Newcastle and North Tyneside 2 under the ethics institutional review board number (IRB) 14/NE/1070 on the 24th of July, 2014. The trial received a clinical trial authorisation from the Medicines and Healthcare products Regulatory Agency (MHRA) on the 9th of September, 2014. Following initial verbal consent in the presence of an independent witness in the cath-lab, written informed consent was obtained from all patients after the PPCI procedure/intervention. Patient samples (serum) were collected at baseline as well as 24 h post-reperfusion. Structural and functional heart assessment was conducted by CMR at median

3 days and 12 weeks post-STEMI. IL-6 serum concentration was measured at both time-points using Luminex-based immunoassay custom by BioRad using IL-6 detection beads of cat#: 171B5006M. The detection limit of the assay is 0.7 pg/ml with Luminex LLOQ. The change in IL-6 concentration (Delta IL-6) was calculated. IL-6R serum concentrations were measured using a commercially available ELISA (DR600, R&D). Patient characteristics as well as CMR-based structural/ functional heart assessment according to Delta IL-6 tertiles are shown in Tables S1 and S2.

Autopsy heart tissues from subjects with acute myocardial infarction (cases) and non-myocardial infarction (controls)/ Rome cohort

Autopsy heart tissues were collected anonymously after a diagnostic autopsy from the histological archive of the Fondazione Policlinico Universitario "A. Gemelli", IRCCS, UOC Anatomia Patologica, Rome, Italy. The inclusion criteria for the cases were autopsy heart tissues where the cause of death was determined by histological diagnosis of acute myocardial infarction with histological signs of ischemia based on standardised criteria as previously reported.[52,53] The inclusion criteria of the controls were subjects that died due to other acute fatal disease than heart disease and for whom the histological analysis of heart excluded a recent myocardial infarction or coronary artery disease. Subject medical histories were used to exclude a previous myocard heart disease in the controls. Death in the five control cases was either due to a massive cerebral hemorrhage or pulmonary embolism. The cold room insulation and the short times before the autopsy ameliorated the effect of self-decomposition or autolytic process in the tissues, as also verified by the autopsy. Both cases and controls were selected by a consecutive cohort of subjects of the same time period who underwent routine autopsy for identification of the cause of death. The autopsy diagnosis was evaluated by a second pathologist (blinded study) in order to confirm the acute myocardial infarction as the cause of death in the cases and exclude it in the controls. The study was approved by the ethics committee of Fondazione Policlinico Universitario Agostino Gemelli IRCCS Università Cattolica del Sacro Cuore, Rome (Italy) under the ethics IRB number 30075/19; 2695. The IHC experiments were performed and analysed without previous knowledge of the group category and were also evaluated by a second experimentator who had no previous knowledge of the autopsy diagnosis per subject.

Chronic ischemic heart disease cohort/ Utah cohort

Patients diagnosed with chronic ischemic heart disease and end-stage heart failure who underwent implantation of a continuous-flow left ventricular assist device (LVAD) as a bridge to transplant or as destination therapy were presented between 2008 and 2014 at the University of Utah Hospitals and Clinics (see also Tables S3 and S4 for patient characteristics). Normal donor hearts that were not allocated for heart transplantation, but due to non-cardiac issues- related reasons, were used as normal controls. All samples were collected with informed consent from patients, organ donors or their guardians. The study was authorized by the University of Utah under the ethics IRB number 00030622 and under the clinical trial registry number NCT01099982. The admission and exclusion criteria, pharmacological therapy as well as further details about the cohort have been previously reported.[54] The protocol for the prospective evaluation of the functional recovery has been developed and applied at the Utah Cardiac Recovery Program, as previously described.[55] For the protein analysis, myocardial tissue and serum samples were immediately frozen in liquid nitrogen and subsequently stored in -80 °C till use. IL-6 in cardiac tissue and serum was measured using Luminex-based Multiplex Immunoassays (Millipore, HSTCMAG28SPMX13). The immunoassay signal was detected using the Luminex 200 Multiplexing Instrument. The intra-assay % coefficient variation is < 5 %. The assay sensitivity range is 0.11-8.17 pg/ml. Equal amount of total protein was used for both patients and controls to ensure that the samples were comparable. The immunoassay signal was recorded using the Luminex 200 Multiplexing Instrument. For the western blot analysis, protein was extracted using a lysis buffer supplemented with protease and phosphatase inhibitors, as described above for the *in vitro* studies. For antibody details see key resources table. Western blots were developed using the ECL Plus reagent (GE Healthcare) and Kodak 6 Biomax MR chemiluminescence film. For the correlation studies, changes of IL6ST and ADAR2 mRNA *vs* pSTAT3/STAT3 levels in the same individuals were only considered.

Animals

All animal experiments were conducted according to the principles of laboratory animal care and to the German laws. The studies have been approved by the ethical committees (Regierungspräsidium) of Darmstadt (Hessen, DE) and Munich (Bavaria, DE). ADAR2 null mice that harbour a knock in (KI) mutation for the pre-edited form of glutamate receptor subunit B (Adarb1$^{-/-}$/*Gria2*$^{R/R}$; named Adarb1$^{-/-}$/KI in this manuscript for simplicity reasons) and the control littermates (Adarb1$^{+/+}$/*Gria2*$^{R/R}$; named Adarb1$^{+/+}$/ KI in this manuscript) were obtained from (allele symbol *Adarb1*^{tm1Phs}) MMRRC. The strain genetic background is B6.129 and was first generated by Peter H. Seeburg (Department of Molecular Neuroscience, Max-Planck Institute for Medical Research, Heidelberg, Germany), as previously described.[3] A conditional Cre/loxP gene deletion strategy was selected to ablate ADAR2 expression from ECs, utilizing a VE-cadherin promoter-driven endothelial Cre recombinase expression.[56] The conditional ADAR2 mice (*Adarb1*$^{flox/flox}$) were kindly provided by Shin Kwak (Tokyo, Japan)[57] and crossed with VE-Cadherin(PAC)-Cre-ERT2 mice,[56] a kind gift from Prof. Ralf Adams, to generate tamoxifen-inducible endothelial-restricted loss-of-function. As controls Adarb1$^{+/+}$/*Cdh5*-Cre$^{ERT2\ tg/0}$ or *Adarb1*$^{flox/flox}$/*Cdh5*-Cre$^{ERT2\ 0/0}$ were used, as no significant differences were observed among these genotypes in the experimental settings during pilot studies following the same tamoxifen treatment scheme as described below (data not shown). Similarly, *Il6st*^{flox} mice[58] (intercrossed with B6.129(Cg)-*Gt(ROSA)26Sor*$^{tm4(ACTB-tdTomato,-EGFP)Luo}$/J; stock no. 007676) were provided by Prof. Christian Trautwein (Aachen University, Germany) and were crossed to the same VE-cadherin(PAC)-Cre-ERT2 mice as the *Adarb1*^{flox} mice. *Adar*^{flox} mice, which were obtained from the Jackson Laboratory (B6.129-*Adar*^{tm1Knk}/*Mmjax*) and generated as previously

described,[1] were also crossed to VE-cadherin(PAC)-Cre-ERT2 mice as the *Adarb1*^{flox} mice (named iEC-Adar$^{-/-}$ in this manuscript). To induce gene ablation, tamoxifen (#T5648, Sigma-Aldrich) was administered intraperitoneally at five consecutive doses (each dose at 80 mg/kg per mouse), as it has been previously determined in literature for these vascular endothelial cell Cre reporter mice.[59–62] All murine experimental procedures described below have been performed one week following the last tamoxifen injection in the respective mice to minimize any potential tamoxifen-related side effects in the experimental studies. All experimental mice (apart from the *Adarb1*/KI) were treated with tamoxifen to ensure that any residual tamoxifen-related effects are present in both control and target animals. Littermate controls were used to account for the diverse genetic background and environmental cues. For the cremasteric microcirculation experiments only male mice were used. For all the rest animal experiments similar numbers from both female and male mice were studied. Genotyping was performed by PCR as previously described[56,57] using the extracted DNA from tail biopsies (RedExtractNAmp kit, Sigma Aldrich).

Primary cell cultures

Primary human umbilical vein endothelial cells (HUVECs), pooled from three donors, were purchased from Lonza and cultured until passage five, as previously described.[18] All cells were tested negative for mycoplasma and authenticated by Lonza. Primary murine endothelial cells were isolated from freshly harvested murine lungs as described before,[63] and where indicated, they were treated with 5 μM of 4-OH tamoxifen (Sigma-Aldrich) for 72 h for tamoxifen-inducible gene ablation. Non-primary murine endothelial cells, H5V, were cultured as previously described.[63]

METHOD DETAILS

In vitro related procedures

Treatments, stimulations and RNA interference knockdown of cultured endothelial cells

Lipofections for transient transfections were conducted as previously described[18] and using the indicated at the figure legends concentrations of siRNAs (nM). A table of the siRNA sequences and assay identifiers used are available in Table S5. Human recombinant IL-6 (10 ng/ml; 206-IL, R&D Systems) was combined with human recombinant IL6Rα (100 ng/ml; 227-SR-025, R&D Systems) in a homogenous mixture of basal EC medium which was distributed uniformly in each experimental cell dish. As a vehicle, DPBS containing 0.1% BSA was utilized. Alternatively, recombinant human IL-6/IL-6Ra protein chimera (8954-SR-025, R&D) at 0.01, 10 ng/ml were used diluted in DPBS containing 0.1% BSA. IL-11 (218-IL-005, R&D), IL-27 (2526-IL-010, R&D), cardiotrophin (612-CD-010, R&D), LIF (7734-LF-025, R&D) or oncostatin M (295-OM-010, R&D) were reconstituted according to manufacturer instructions. Cells were incubated for the indicated times in the figure legend of Figure 1. For the phosphorylation STAT3 western blot of the phenocopy studies cells were stimulated for 30 min. Evaluation of previously described IL-6-trans-signalling-induced inflammatory mediator (E-selectin, ICAM-1, MCP-1, VCAM-1) expression[26,64] were used to monitor the stimulation index. Experiments with similar and positive stimulation index were taken into account. Regarding the hypoxia experiments, immediately before the cell dishes were inserted into the hypoxic chamber, the medium was removed and fresh pre-equilibrated (for 6 h) hypoxic medium (1% O_2 in a Labotect C16 CO_2/O_2 incubator from Labor-Technik-Göttingen GmbH or a HypoxyLab^{TM} incubator from Oxford Optronix Ltd, UK) was added. Cells were incubated for additional 24 h. The control cell dishes which were incubated under normal oxygen conditions received basal medium and continued to be incubated for additional 24 h in a regular cell incubator. VEGF expression was monitored after cell lysis to verify the induction of hypoxia. Only the experiments in which VEGF expression was induced were included in these studies.

RNA isolation, quantitative SYBR-, and TaqMan- RT-PCR

Total RNA preparations performed using either the miRNeasy Mini kit (Qiagen) or the Direct-zol RNA MiniPrep kit (Zymoresearch) according to the suggested manufacturers' protocols. Both were coupled with DNase digestion (Qiagen or Zymoresearch) to remove genomic contamination prior to cDNA synthesis and PCR. The quantity of the recovered RNA was documented by Nanodrop 2000/3000 (ThermoScientific). Reverse transcription was performed by MuLV reverse transcriptase (ThermoFisher Scientific) for both standard gene expression and primary miRNAs quantification. The cDNA was subjected to quantitative SYBR Green real time PCR (StepOnePlus & Fast Green Mastermix or QuantStudio 7 & PowerUP SYBR Green Master Mix; both from Applied Biosystems) for standard gene expression. Alternatively, for primary miRNAs quantification, pre-designed TaqMan probes by ThermoScientific were employed. Gene expression data were
normalized to RPLP0 (standard gene expression) or TBP (TaqMan-based qPCR) mRNA levels. With respect to mature miRNAs quantification, pre-designed TaqMan miRNA assays were employed for each case and U6 was used as a housekeeping gene corresponding to the average length of mature miRNAs. StepOne Plus or ViiA 7 RT PCR System (both by Applied Biosystems) were used for all the measurements. QRT-PCR measurements were performed in two technical replicates per independent biological sample tested. The relative expression levels were determined using the formula $2^{-\Delta Ct}$ ($\Delta Ct=Ct_{(gene\ of\ interest)}-Ct_{(housekeeping\ gene)}$). The primers and TaqMan probes used are available in Table S5.

Overexpression studies

The human ORFs of ADAR2 and IL6ST with registry number NM_00112/NP_001103 and NM_002184, respectively, were cloned into a pCMV6-Entry vector (RC209073, Origene) using SgfI-RsrII restriction sites. For the generation of the ADAR2 catalytically inactive construct, a point mutation E396A was introduced into the ADAR2 ORF. HUVECs were transfected with ADAR2 expressing (ADAR2^{OE}), an ADAR2 editing-deficient (ADAR2 E/A^{OE}) expressing or control (empty) construct for 72 h. Both the unedited and

the pre-edited pri-mir-199a1 and pri-mir-335 constructs were generated by inserting the human DNA fragment which corresponds to each pri-miRNA hairpin, flanked by 200 nucleotides in either side of the hairpins, into pcDNA 3.1 (+) plasmid (Invitrogen) using the NheI and EcoRV restriction sites. With regards to the pre-edited constructs, the inserts of the unedited pri-miRNA fragments were point mutated A-to-G at the corresponding editing sites, as depicted in Figure 7H. All plasmids bear the cytomegalovirus (CMV) immediate early promoter suitable for replication within mammalian cells. 0.1 μg of either *ADARB1*-pCMV6-Entry, *ADARB1 E/A*-pCMV6-Entry, *IL6ST*-pCMV6, pCMV6-Entry, unedited pri-mir-199a1-pcDNA3.1, unedited pri-mir-335-pcDNA3.1, pre-edited pri-mir-199a1-pcDNA3.1 and pre-edited pri-mir-335-pcDNA3.1 were utilized as determined by preliminary titration experiments. Each construct was introduced to HUVECs seeded one day before using Lipofectamine 2000 (Invitrogen) following manufacturer's recommendations as described.[18] As a control, the empty pCMV6-Entry vector (Origene) vector was used.

Immunoblotting analysis

For determination of protein expression, HUVECs were lysed and equal amounts of protein (50 μg/lane) were loaded onto a SDS-polyacrylamide gel and blotted onto polyvinylidene difluoride (PVDF) membranes (Immobilon PVDF membranes, Sigma Aldrich), as previously described.[18] Western blotting was performed using antibodies listed in the key resources table. Enhanced chemiluminescence was performed according to the manufacturer's instructions (Amersham, Freiburg, Germany). Images were acquired by the FluorChem M FM0259 Digital Room (Proteinsimple, California, USA) or the ChemiDoc Imaging System (Biorad, Berkeley CA, USA). The blots were re-probed with an antibody against α-tubulin as loading control, after a short incubation of the membrane with Restore Western blot Stripping Buffer (ThermoScientific).

ELISA-based assay

Proteins were profiled using Luminex-based Multiplex Immunoassays (Human Cytokine /Chemokine Panel; Cat no: HD71 or Mouse Cytokine/Chemokine Panel; Cat no: MD44, Eve Technologies, Alberta, Canada).

Leukocyte static adhesion assay

For *in vitro* adhesion assays, human freshly isolated leukocytes obtained from healthy donors were isolated by Ficoll-based density gradient centrifugation (Biochrom, Merck) as described[18] Thereafter, leukocytes were visualized with Rhodamine 6G (R4127, SigmaAldrich) staining and allowed to adhere for 30 min onto a monolayer of HUVECs[65] previously transfected with siADAR2 or scrambled control for 48h, and stimulated for additional 6 hours with human recombinant IL-6 (10 ng/ml, R&D) and sIL-6Ra (100 ng/ml; R&D) in a 96-well. After two gentle washing steps with PBS (Gibco), residual adherent leukocytes were visualized and counted by a computer-assisted Axiovert 100 M inverted microscope equipped with a Plan-NEOFLUAR objective (at 5x/0.30) (all from Carl Zeiss, Jena, Germany) as well as analyzed using Axiovision 4.9.1 (Carl Zeiss, Germany) software.

IL6ST mRNA stability assay

The stability of *IL6ST* mRNA was measured after inhibiting the transcription using actinomycin D (A1410, SigmaAldrich) during a time-course assay as previously reported.[18]

Luciferase reporter activity assay

The luciferase *IL6ST* 3′UTR construct was prepared by inserting the synthetized (Eurofins) entire *IL6ST* 3'UTR (5985bp) sequence which was obtained by UCSC database (hg38) into the psiCheck2 vector (Promega) and flanked by firefly and renilla luciferase. An established protocol for adherent primary cells[18] was set in the Electroporation system Neon™ (Invitrogen, Darmstadt) to introduce the plasmid into HUVECs. The activity of firefly and renilla luciferase was quantified after 24 h using the Dual-Luciferase Reporter 1000 Assay System (Promega) according to the manufacturer's protocol in a GloMax®-Multi+ Microplate Multimode Reader (Promega).

Precursor and LNA miRNAs studies

Precursor miRNAs or precursor Negative control (in total 10 nM per reaction) were introduced to HUVECs using the lipofection approach which was described for the siRNAs above. Seventy-two hours post-transfection, HUVECs were harvested for qRT-PCR analysis. Alternatively, 48 h later HUVECs were electroporated to receive the *IL6ST* 3'UTR construct and subjected to luciferase reporter assay 24 h later. For the rescue experiments, 24 h after seeding, HUVECs were transfected with the indicated siRNAs and 48 h later the complexes lipofectamine- LNA miRNAs or LNA negative control (50 nM per reaction) were also introduced to the cells and allowed to be incubated for 24 h further before harvesting (72 h since the siRNA transfection). Transfection efficiencies had been monitored by TaqMan-based qRT-PCR studies and only those experiments with sufficient overexpression (> 50 %) or knockdown of miRNA (> 70 %) expression were considered. Specific details on the used assays are available in Table S5.

High-throughput deep small and total poly-A RNA sequencing (RNA-seq)

Prior to processing RNA quality was certified by 2100 Bioanalyzer (Agilent Genomics). Small RNA sequencing libraries were prepared using TruSeq small RNA kit, as previously described in detail.[66] The libraries were sequenced using the Illumina HiSeq 2000 for 1 x 51cycles standard protocol. The total poly-A RNA sequencing data were obtained from Stellos et al.[18]

Bioinformatics analysis of expression and RNA editing of miR-sequencing data

For the miR expression bioinformatics analysis, the mapping of miR-sequencing reads, variant calling and filtering were performed as previously described.[67] MiR-seq-based RNA editing analysis and quantification was performed as described.[68,69] For the venn diagram in Figure 6C, the human and murine targetome of the candidate miRs provided by a web-based tool (MiRWalk 2.0; http://zmf.umm.uni-heidelberg.de/apps/zmf/mirwalk2), which additionally combines the data of three well-known databases (miRanda, RNA22, Targetscan), cross-referenced with the at least 4-fold downregulated transcripts after ADAR2 knockdown reveals two common denominators across the three lists, *IL6ST* and *LIMCH1*. Due to low replicate number of the miR-seq (n = 3) differentially expressed candidates with $P \leq 0.1$ *vs* scrambled were taken into consideration.

Sequences alignment and counts generation of the IL-6/basal ADAR2-deficient EC ribo-zero total RNA-seq

The obtained fastq files were trimmed for Illumina adapters using Cutadapt[70] version 2.10 and subsequently passed quality control using FASTQC[71] version 0.11.9 and MultiQC[72] version 1.9 tools. The trimmed and quality checked reads were then aligned to human genome GRCh38.p13 from Ensembl[73] using STAR[74] aligner version 2.7.0e-foss-2018b and Ensembl[73] GRCh38.99.gtf annotation file. The generated.bam files were then used as input for htseq-count,[75] with parameters -f bam -a 0 -s no -t exon, to produce tab delimited tables of read counts for each gene.

Differential Gene Expression Analysis (DGEA)

DEA was performed by DESeq2[76] R package from Bioconductor version 3.11 using Rstudio version. 1.2.5033 and R language version 3.6.3. The count tables were read into R using the DESeqDataSetFromHTSeqCount function (default settings) and the appropriate design of the DESeq data set was applied to take into account all samples from all conditions. This was to ensure that normalized counts of the same gene are comparable between different conditions and also to generate a single object with all samples/conditions normalized among each other. At the next step, using the "DESeq" function (default settings), the DESeq object was generated based on which results were produced as output file describing each comparison. Statistically significant genes (Benjamini – Hochberg corrected p-value < 0.05) had a mean of normalized counts > 10. Therefore, genes with mean of normalized counts ≤ 5 where filtered out. Genes with a Benjamini – Hochberg corrected p-value of < 0.05 and a fold change of at least ±1.5 (Log2FoldChange of ±0.58) were considered as significantly deregulated.

Gene Ontology (GO) and Ingenuity Pathway Analysis (IPA)

Gene ontology analysis of the 4-fold ADAR2 regulated genes (provided as input), based on the data derived from high throughput poly(A)-RNA sequencing analysis, was performed using the web-based tool (https://david-d.ncifcrf.gov/; v.6.7) and applying the following criteria (GOTERM_BP_FAT as selected terms and displayed terms with > 6 counts in a functional annotation chart). The Ingenuity Pathway Analysis® tool from QIAGEN®[77] was used to perform an advanced Gene Ontology analysis of the differentially expressed genes. As an input for the IPA®, a list of genes with a corrected p-value of < 0.05 and the corresponding Log2FoldChange was used. We performed the Canonical Pathways analysis using the default settings. To create the final dot plot graphs in R package, the terms "Canonical Pathways" that had a z-score of either < -1 or > 1 and the top-ranking terms are shown.

RNA immunoprecipitation

RNA-immunoprecipitation (RIP) studies were performed as described[18] using the MagnaRIP™ Kit according to the manufacturer's protocol (Millipore) after a short step of 0.1 % formaldehyde (Roth) crosslinking of HUVECs on ice. Details on the antibodies are available on the key resources table.

PCR-based miRNA editing studies

The detailed sequences corresponding to the precursor miRNAs region were obtained from the database http://www.mirbase.org/.[78] The reverse transcription was mainly based on our previously described protocol[18] by integrating a pre-amplification step which utilizes pri-miRNA-specific (RT) primer, instead of random or oligo[dT] primers, as previously suggested.[79] For primer design sequences, refer to Table S5.

Strategy for PCR-based miRNA editing studies primer design

The general considerations of this method have been previously described.[79] Briefly, the pri-mir-specific RT primer (one per tested pri-miRNA) in the vicinity (~200 nucleotides) of the 3'end of the region which is processed to give rise to the precursor miRNA, while the pri-mir-specific PCR primers are designed to flank the 60-70 nt long precursor miRNA region by ~50-150 nucleotides upstream or downstream (in respect to the directionality of the transcription of each gene). Hence, the presence of additional RNA editing sites throughout the extensively long pri-miRNA transcripts cannot be excluded. The PCR product was cleaned-up and subjected directly to Sanger sequencing. The obtained chromatograms were compared with the reference genome obtained by *UCSC* (hg38) and RNA editing rate was quantified as previously described.[18]

In vivo models and related procedures

Immunophenotyping

For the tissue preparation, age- and sex- matched mice were anesthetized and thymus, spleen, lymph nodes and bone marrow were harvested and directly placed in prefilled falcons with chilled PBS (with 2 % FCS) on ice. Tissues were further processed by gently meshing them through 40 μM cell strainers (BD Biosciences) to achieve single cell suspensions. Spleen cell suspensions were further subjected to lysis of red blood cells using ACK solution. Cell counts of single cell suspensions were determined using a Neubauer chamber after instant labelling with Trypan Blue (Gibco, #I5250-061). For multicolour FACS staining, $2.5x10^6$ cells per sample (per organ and mouse) were used. After transfer to 96- well V-bottom plates, cells were incubated with Fc blocking solution (eBiosciences) for 15 min on ice, to avoid any unspecific binding of labelled antibodies. Afterwards, cell suspensions were incubated with a combination of up to 7 anti-mouse antibodies (B220, CD4, CD8, CD11b, CD19, CD25, CD44, CD62L, CD90.2, CD138, F4/80, Foxp3, IgM, Ly6C, Ly6G, NK 1.1, TCRβ, TCRγδ) and in conjunction with a viability dye (Fixable Viability Dye eFlour 450/506, Invitrogen; 1:1000) to enable the quantification of the immune cells per hematopoietic organ and mouse.[80,81] For the intranuclear staining of Foxp3, fixation, permeabilization and staining were performed according to manufacturer's protocol (Transcription Factor Staining Buffer Set, eBioscience). Samples were acquired with a FACSCanto II flow cytometer (BD Biosciences) and further analyzed using FlowJo software. For analysis, leukocytes were selected according to their FSC and SSC properties, and then further pre-gated for single cells (exclusion of duplets) and viability dye-negative events. One investigator was assigned for the cell counting during the

sample preparations to exclude interindividual differences. The investigators were blinded to the animal genotype. The antibodies are listed in the key resources table.

Intravital microscopy of the cremasteric muscle microcirculation

To assess the EC-leukocyte interactions *in vivo*, intrascrotal injection of 1 μg recombinant murine IL-6/IL-6Rα protein chimera (hyper-IL-6; 9038-CF, R&D) or equivalent PBS volume per mouse was used to induce IL-6 trans-signalling-dependent inflammatory responses. Male mice compared were of similar weight and of 10-14 week-old age. For ischemia-reperfusion experiments, the feeding artery was clamped for 30 min. To record the activities of the myeloid cell subsets through the post-capillary venules of the cremaster, the cremaster muscle was surgically exposed four hours later and an Olympus BX51 microscope equipped with a Hamamatsu 9100-02 EMCCD camera (Hamamatsu Photonics) and a 20x water-dipping objective was used. The labelling of myeloid cell subsets was achieved by injection of antibodies to Ly6G, Ly6C and CD11b, 10 min prior to visualization.[82] To study the adhesion molecule expression, the carotid artery of anaesthetized mice was cannulated for both antibody injection (E-selectin blocking Ab, 9A9, InVivo) and blood sampling (ProCyte Dx; IDEXX Laboratories) and the cremaster muscle was dissected four hours later. Intravital microscopy was conducted on a Zeiss Axio Examiner.D1 microscope, equipped with a 40x objective (Zeiss, 0,75NA, water immersion objective) and an Axiocam 702 camera. Number of rolling and adherent cells mm^{-2} were analyzed in post-capillary venules and leukocyte rolling velocities were determined, before and after E-selectin antibody injection, as well as vessel diameter and vessel length.

To study the blockade of IL-6 trans-signalling, intrascrotal injection of soluble gp130Fc or PBS control was performed 5 min before the clamping of the feeding artery for 30 min. Four hours later, the cremaster muscle was exteriorized and intravital microscopy conducted on a Zeiss Axio Examiner.D1 microscope, equipped with a 40x objective (Zeiss, 0,75NA, water immersion objective) and an Axiocam 702 camera. The key resources table contains further details on the antibodies used in the studies.

Immunostaining of murine cremaster muscles

To study adhesion mediators of IL-6/IL-6Rα or PBS treated mice, whole-mount staining of PFA fixed cremaster muscles was performed. Sex- and age- matched C57BL/6 and *Adarb1*/KI mice of 10-14 week old were used. First, goat-α-rat-AlexaFluor 546 secondary antibody (2 μg mL^{-1}, Invitrogen) staining against E-selectin was conducted for 1 h at RT and then tissues were stained with AlexaFluor 488 conjugated rat-α-VCAM-1 and AlexaFluor 647 conjugated rat-α-ICAM-1 for 3 h at RT. Finally, samples were embedded in Mountant PermaFluor aqueous mounting medium (Thermo Scientific) and imaged by confocal microscopy at the core facility Bioimaging of the Biomedical Center with a Leica SP8X WLL microscope equipped with a HC PL APO 40x/1.30 NA oil immersion objective. Three-dimensional (3D) stacks were recorded and images were processed and analyzed using FIJI software, normalizing the mean fluorescence intensity of each stack to the vessel area. The key resources table contains further details on the antibodies used in the studies.

In vivo *hyper-IL-6-induced peritonitis*

To evaluate the leukocyte transmigration through the vascular endothelium of all the strains described above at the section "Animals", we used the sterile peritonitis model, as previously described.[82] Briefly, a single dose of hyper-IL-6 (1 μg/mouse) was administered intraperitoneally to sex-matched, littermate mice of 10-14 week-old for 4 h. All experimental mice compared were of similar weight. Upon completion of 4 h, mice were anesthetized and 5 ml of cold Hanks Balanced Salt Solution (HBSS) was injected into the peritoneal cavity with a 27 G needle. Mice were swished during 3 min and 2 ml HBSS was retrieved with a 26 G needle. Blood and bone marrow samples were lysed with erythrocyte lysis buffer (Biosciences). Peritoneal lavage samples were not subjected to erythrocyte lysis buffer treatment since they were inspected visually for erythrocyte presence (reddish colour of sample) which would indicate abnormal blood leakage into the peritoneal cavity. One ml of the recovered peritoneal lavage as well as blood and bone marrow samples stained with antibodies against CD45, CD11b, Ly6G (Gr1), CD115, and leukocyte populations were analyzed by flow cytometry. The flow cytometry experiments were recorded using Fortessa X20 (BD). Further information on the specific antibodies used is listed in the key resources table and on the specific genotypes tested in the corresponding figure legend of Figure 2. Absolute cell numbers were assessed by use of CountBright™ absolute counting beads (Invitrogen). Peritoneal lavage content, whole blood and bone-marrow samples, all taken simultaneously from the same mice to allow direct comparisons, were processed.

Murine myocardial infarction model (MI)

Ischemia was induced by permanent ligation of the left anterior descending artery (LAD) in sex- and age- matched adult mice of 10-12 weeks, as previously described.[83] Cardiac MRI (magnetic resonance imaging) measurements were performed as previously described[83] utilizing a 7.0 T Bruker PharmaScan, equipped with a 375 mT m^{-1} gradient system, equipped with a custom-built circularly polarized birdcage resonator and the Early Access Package for self-gated cardiac imaging (Intragate, Bruker), before (pre-MI) and after (post-MI) the operation to objectively monitor the cardiac function with high sensitivity by quantifying the left ventricular ejection fraction (LVEF) before and one week after ligation. The ischemic heart disease was categorized as mild when the LVEF > 45% (after distal LAD ligation) or severe when the LVEF < 35% (after proximal LAD ligation). The number of operated animals is provided in the figure legend of Figure S6. Hearts from humanely killed animals were cryo-embedded in OCT compound. The heart tissues of day 28 after myocardial infarction were sectioned in the left ventricle transverse direction from the ligation level down to the apex. Cryosections were cut at 10 μm tissue thickness per section from 3 different anatomical levels (500 μm thickness intervals) per heart. Masson's trichrome staining (ab150686, Abcam) was performed according to manufacturer's instruction to quantify fibrosis area in the left ventricle. Three to five images per heart were acquired using DMi8 THUNDER imager (Leica). Left ventricle fibrosis area and total left ventricle area of each image were measured with Image J software, and fibrosis area was expressed as a percentage of the total left ventricle area. Cryosections were permeabilised using 0.3 % Triton in PBS for 30 min and incubated with 1 % BSA in PBS for 30 min at room temperature followed by incubation with either anti-CD45, rat anti-mouse VCAM-1 or hamster anti-mouse

MCP-1 overnight at 4°C or incubation with either the primary rat anti-mouse CD62E or hamster anti-mouse ICAM-1 in HEPES buffer for 1 h at room temperature. After washing with PBS thrice for 5 minutes each, the sections were incubated with secondary antibody conjugated to Alexa 488 or 568 for 2 h at room temperature. For the adhesion molecule immunostaining studies, counter-staining of these tissues was performed with the primary rat anti-mouse CD31 followed by the secondary antibody goat anti-rat Alexa 568. Following three additional washing steps with PBS, the sections were mounted with Prolong Gold with DAPI (P36935, Thermofisher) to identify nuclei and prevent fluorescence quenching. Images from 10 high power fields (hpf) within the infarcted zone were acquired per heart using DMi8 THUNDER imager (Leica). The number of $CD45^+$ cells per hpf was quantified using LAS X software (Leica) and the average $CD45^+$ cell counts were calculated per ten hpf for each mouse. Quantification of the intensity of adhesion molecule expression was performed using ImageJ software (v1.52p). The ratio of primary antibody and CD31 intensity was calculated. Details for antibody concentrations see key resources table.

Murine ischemic hindlimb model

The hind limb ischemia was inflicted by ligation of the superficial and deep femoral artery and vein of the right leg, and the blood flow was measured by a laser Doppler blood flow meter (Laser Doppler Perfusion Imager System, moorLDI-Mark 2, Wilmington, DE) as previously described.[84] Sex- and aged- matched adult mice at the age of 10-12 weeks were used. The number of mice is provided in figure legend of Figure 3. The murine operations and the sample preparations were repeated three times at three distinct days. Each day equal numbers of control and target animals planned to be tested. Sample power per group was determined by the breeding outcome and littermate controls were used. Animals that either died during anaesthesia or did not exhibit sufficient ischemic index were excluded from the investigation.

Immunostaining of murine hindlimb ischemia tissues

Cryo-sections of 10μm-thickness snap-frozen ischemic muscle tissues were stained after standard preparation procedures.[84] Briefly, for the assessment of leukocyte cell infiltration within the ischemic regions by CD3 and Ly6G counterstained with CD45 and DAPI and counts were determined per nuclei (DAPI) and CD45 positive cell number. For the adhesion mediator expression, immunostaining studies were performed as described above in the MI tissue section. For details regarding the antibodies see key resources table.

Absolute quantification of immune cell trafficking in murine hindlimb ischemia model

Flow cytometry analysis of immune cell infiltrates in muscles, was performed as previously described.[85] Briefly, ischemic and non-ischemic muscles were digested using the Skeletal Muscle Dissociation Kit and gentleMACS (Miltenyi Biotec). Following red blood cell lysis, single cell suspension derived from muscle was stained with fluorochrome-conjugated antibodies (all from BioLegend): BV510-conjugated anti-CD45, PE-conjugated anti- Ly6G, APC-conjugated anti-CD11b, FITC-conjugated anti-Ly6C, BV421-conjugated anti-F4/80, PE/Cy7-conjugated anti-I-Ab (MHCII), APC/Cy7 anti-CD3, APC/Cy7-conjugated anti-CD45R/B220, and APC/Cy7-conjugated anti-NK1.1 ('Lineage' channel). 7-AAD (BioLegend) was used to distinguish living from dead cells. Parallel addition of AccuCount Rainbow Fluorescent beads (Spherotech, Inc, Fulda, Germany) allowed the absolute quantification of infiltrated cells by flow cytometry. Data acquisition was performed on a BD FACSCanto II flow cytometer using FACSDiva software (BD). The analysis of acquired data was performed using FlowJo software (Version 10 for Macintosh, Tree Star, Inc.). Two-dimensional plots (pseudo-colour or zebra) were created using bi-exponential transformation, and sequential gating of leukocyte subsets was performed as shown in Figure S5F.

Postnatal retinal angiogenesis model

Mice were sacrificed at postnatal day five (P5) and their eyes were retrieved and processed similarly to a previously described protocol.[56] Antibody information is available in key resources table.

Human tissue studies

Immunohistochemistry for human cohorts (Rome and Utah Cohort)

Formalin-fixed, paraffin-embedded sections (3 μm thickness) were mounted onto positive charged glass slides. Serial sections were baked for 60 minutes at 56° C in a dehydration oven. Antigen retrieval and deparaffinization were carried out on PT-Link (Dako) using the EnVision FLEX Target Retrieval Solution kits at low pH (Dako), as manufacturer's instruction. Following unmasking protocol, endogenous peroxidases were blocked for 5 minutes with 3% hydrogen peroxide (Sigma), then washed twice at RT in a specific buffer (Dako) and incubated for 30 minutes with 5% PBS/BSA. Sequential slides were then incubated overnight at 4°C with primary antibodies: anti-ADAR2, anti-CD31, anti-CD45-LCA, anti-IL6ST and anti-CD43, respectively. Secondary antibody (EnVision FLEX/HRP) coupled with peroxidase (Dako) for 20 minutes RT. Bound peroxidase was detected with diaminobenzidine (DAB) solution and EnVision FLEX Substrate buffer (Dako). Tissue sections were counterstained with EnVision FLEX Haematoxylin (Dako). See key resources table for further details on antibodies.

Immunoreactivity Score

Tissue slides immunostainings were evaluated and graded by an experienced pathologist, who was blinded to the clinical data and the other manuscript data and message. In order to assess any differences in ADAR2 expression between normal and diseased tissues, a scoring system was applied. Specifically, ADAR2 nuclear expression was semi- quantified using an immunoreactivity score which was calculated as the percentage of high-intensity ADAR2 expressed vascular endothelial cells over the total CD31-positive endothelial cells per high powerfield (range 0-100%).

QUANTIFICATION AND STATISTICAL ANALYSIS

Statistical analysis for clinical data

Normality of continuous variables was graphically assessed by histograms and P-P plots, as well as by Kolmogorov-Smirnov test. Differences between controls and cases were assessed by independent samples t-test for continuous variables or Mann-Whitney *U* test, when normal distribution did not apply. Chi-square test was used to examine differences in categorical variables. Correlations between variables were evaluated using Pearson's correlation coefficient, unless otherwise stated. No statistical method was used to predetermine sample size. No samples were excluded from the analysis. Experiments were not randomized. Investigators were blinded to patients' clinical or experimental data. We deemed statistical significance at a = 0.05.

Statistical analysis for *in vivo* data

Data are either presented in bar graphs as mean ± s.e.m. or in box plots (box plot line (from top to bottom): maximum; Q3, third quartile; median; Q1, first quartile; and minimum). Two experimental groups were compared using a two-tailed non-parametric Mann-Whitney *U*-test or t-test depending on data distribution. *P-value* < 0.05 was considered as significant. No statistical method was used to predetermine sample size. Only mice underwent successful operation exhibiting reduced blood perfusion after ligation were considered for the analysis of the hindlimb ischemia model. Experiments were randomized. Investigators were blinded to the genotypes of the mice.

Statistical analysis for *in vitro* data

Data are presented in bar graphs as mean ± SEM unless otherwise stated. Two experimental groups were compared using a two-tailed non-parametric Mann-Whitney *U*-test or t-test depending on values distribution. *P-value* < 0.05 was considered as significant. In order to account for multiple comparisons, Bonferroni correction was performed where applicable. No statistical method was used to predetermine sample size. Only samples with sufficient stimulation index, knockdown or overexpression efficiency and hypoxic index were considered for the analysis. Experiments were randomized and analysis blinded to the genotype.

ADDITIONAL RESOURCES

This study has used a subcohort of the CAPRI trial with registry number: NCT02390674 and the Utah trial with registry number: NCT01099982.